GEORG-AUGUST-UNIVERSITÄT
GÖTTINGEN

FAKULTÄT FÜR PHYSIK

BACHELOR'S THESIS

Classifying nonequilibrium steady states via invariant manifolds

Klassifizierung von Nicht-Gleichgewichtszuständen mittels invarianten Mannigfaltigkeiten

Jens Lucht

jens.lucht@stud.uni-goettingen.de

Advisor & First Referee: **Dr. Marco G. Mazza**

Second Referee: **Prof. Stefan Klumpp**

15. February 2018

Max Planck Institute for Dynamics and Self-Organization

Dynamics of Complex Fluids, Nonequilibirum Soft Matter

Abstract

Nonequilibrium steady states (NESS) give rise to nontrivial cyclic probability fluxes that breach detailed balance (DB), and thus it is not clear how to define a potential analog to the equilibrium case. In this thesis we argue that possibly there is a formal way to define such a NESS potential for systems describable by a Fokker-Planck equation. DB in NESS can be restored [1] by mapping the phase space into a parameterized family of non-intersecting cycles containing the invariant manifolds of the corresponding deterministic, dynamical system. Transition rates between neighboring cycles are obtained from the microscopic dynamics, i.e., from the drift and diffusive currents. Since fluxes between cycles obey DB, we can integrate over the set of cycles. We present some evidence that this gives us a nonequilibrium potential which reaches minimum solely for NESS.

The main goal of this thesis is to put forward a tentative theory for deriving a generalized potential function whose extrema identify the NESS. We will present results of a first numerical test based on two well-known dynamical systems: the van-der-Pol oscillator and the Brusselator. Our results, although not conclusive, are encouraging.

Contents

Chapter 1

Introduction

In nature equilibrium is more the exception than the rule [2]. Many systems we encounter everyday are far from equilibrium and show eye-catching patterns and collective behavior. Some well-known examples are swarming of starling or fish schools [3], swimming bacteria [3–6], clustering in cosmic dust [7], thermal convection of a hot liquid in a coffee cup [8], and even traffic jams [2]. Collective behavior arises from the interaction of many similar *units*, for example molecules and birds in flocks, whose individual interactions become dominated by the influence of the others, *collectively* interacting [3]. Some examples are shown in Figure 1.1. A non-zero flux of energy or matter is observed as characteristic for nonequilibrium systems, for example the constant pumping of a laser [9] or glucose in the glycolytic cycle [10]. Despite their omnipresence a framework for theoretical description is still missing [11]. Providing a nonequilibrium counter-part to the well understood equilibrium physics has become one of the greatest challenges in modern statistical physics [11–13]. Such a framework may provide (new) insights into many fields, for example, the glycolytic cycle, which is even at the basis of our life[1], population dynamics or active biological systems.

Nonequilibrium has different origins and systems can be grouped into equivalence classes based on the underpinning mechanism [5]. The first class are systems that are still relaxing towards equilibrium but have not yet reached it. The speed of relaxation can take arbitrary values down to extremely slow as for glasses. Systems in the second class have boundaries through which fluxes of energy or matter establish nonequilibrium conditions. A very simple example for this is a system coupled to two reservoirs at different temperatures implying a non-zero heat-flow through our system. We might say the system is subject to external driving. Note that such systems do not posses an equilibrium state where all fluxes vanish, because such state cannot satisfy the boundary conditions. The third class is represented by the so-called *active matter*, which dissipates energy at the lowest dynamical level of the

[1] ... and the annoying traffic jams during our daily trip to work

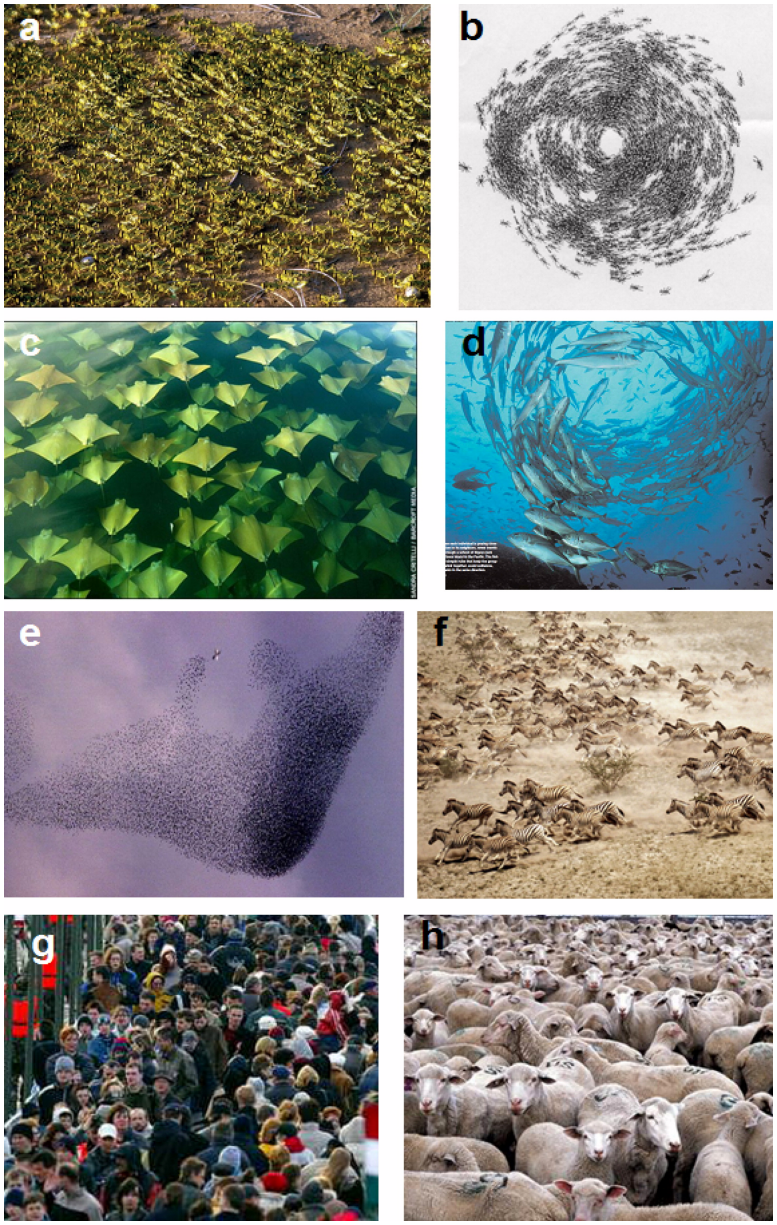

Figure 1.1: Gallery of collective behavior in biological systems. Interaction among individual *units* is dominated by integration of groups (*collection*). These systems are examples of *active matter*, which constantly converts (free) energy into directed motion and hence is not in equilibrium [4]. (a) Wingless locusts marching in the field. (b) A rotating colony of army ants. (c) A three-dimensional array of golden rays. (d) Fish are known to produce such vortices. (e) Before roosting, thousands of starlings producing a fascinating aerial display. They are also trying to avoid a predator bird close to the central, finger-like structure. (f) A herd of zebra. (g) People spontaneously ordered into "traffic lanes" as they cross a pedestrian bridge in large numbers. (h) Although sheep are known to move very coherently, just as the corresponding theory predicts, when simply standing (no motion), well developed orientational patterns cannot emerge. Images taken from [3].

individuals. Such dynamics are irreversible by design. An example is the beating flagellum of swimming bacteria.

In this thesis we start by reviewing the current framework to describe *nonequilibrium steady states* (NESS) with focus on concepts necessary to explore a candidate ansatz for a NESS potential. Therefore we will address the following key questions:

(i) What distinguishes equilibrium from nonequilibrium stationary states?

(ii) How are these states reached? And what are the underlying dynamics?

(iii) Can we give a general method for classifying NESS?

The main goal of this thesis is to put forward a tentative theory for deriving a generalized potential function whose extrema identify the NESS. In the remaining part of this introduction we will outline a thermodynamic description to compare equilibrium and NESS. In Chapter 2 we will review the for our course needed concepts of dynamical systems theory and stochastic dynamics. Afterwards, in Chapter 3 we introduce our candidate ansatz for a NESS potential. We focus on the numerical aspects in Chapter 4 and present our results for two dynamical systems in Chapter 5. Finally, a discussion follows in Chapter 6.

1.1 Equilibrium versus nonequilibrium

Before we explore the rich and stunning phenomenona of nonequilibrium, we should review what we call an equilibrium state and how we describe it with thermodynamics. In thermodynamics equilibrium is governed by *extremal principles*. On the one hand, for isolated systems the entropy is maximized. On the other hand, for systems coupled to a reservoir the principal of minimum energy leads to a definition of equilibrium: an equilibrium state minimizes a thermodynamic potential. For instance a system coupled to a single reservoir, held at a constant temperature T and volume V, equilibrium is reached if (and only if) the Helmholtz free energy F is minimized. Hence it is called thermal equilibrium. If other quantities are held constant other potentials are minimized. Some well-known potentials are the Gibbs free energy, enthalpy and internal energy [10, 14].

In our phenomenological understanding, equilibrium is time-independent and spatially uniform. This enables us to use only a few *macroscopic* observables, which completely characterize our equilibrium distribution. Macroscopic measurements are performed at time and length scales much larger than the atomic scale. We might see this as coarse-graining in space and time. During measurement, the particles undergo rapid (compared to macroscopic timescales) and complex motions. This atomic view is known as *microscopic* description, where each particle is taken into account. Macroscopic observables are for example pressure, volume and internal energy [14, 15].

We note that equilibrium states arise as a relaxation in the long-time limit because systems in general have a tendency to reach equilibrium [14]. The length of the

relaxation can be different, depending on the initial configuration, but equilibrium does not depend on the initial configuration [11].

A system being at or close to thermal equilibrium is successfully described by the Boltzmann-Gibbs framework. As inputs it requires a set of possible states s_i–the *mircostates*–and an expression for the internal energy, given by a Hamiltonian $\mathcal{H}(s)$ for each configuration. Finally, given a temperature T we can write the stationary distribution $p^*(s) = Z^{-1} \exp[-\beta\mathcal{H}(s)]$, where $\beta \equiv 1/k_B T$ is the inverse temperature, k_B the Boltzmann constant and Z is the partition function, given as sum over all states. In many cases the partition function is difficult to compute or even inaccessible [11].

We are now ready to answer question (i). For homogeneity in space and time to hold the distribution of states cannot depend on either of them. Therefore *no net fluxes*[2] *can be present in equilibrium.* This concept is known as *detailed balance* (DB) and states: each possible transition between two states is balanced by its reverse [16]. In other words the flux from state A $\to$ B, r_{BA}, is equal to its reverse flux B $\to$ A, r_{AB},

$$r_{BA} = r_{AB}. \tag{1.1}$$

This is a strong statement and enables us to define potentials [7, 11, 17, 18]. We will have a closer look to its implications in Section 2.3.4.

The balance of fluxes between all states to satisfy DB condition requires *reversibility* of the equations of motion, which is known as *microscopic reversibility.* It is related to the time invariance of the microscopic equations [11]. In thermodynamics, the distinction between reversible and microscopic irreversible processes is manifested in the second law of thermodynamics, which assigns zero entropy change only for reversible processes.

In NESS however there are non-vanishing steady fluxes and *detailed balance is breached.* Hence macroscopic descriptors φ are not spatially homogeneous $\varphi = \varphi(x)$. Due to this fact, we are unable to define a NESS potential, that gains a minimum only in NESS. As counterpart to extremal Helmholtz free energy in thermal equilibrium.

To define a potential for NESS many attempts have been made. Some of them based on *entropy production* to be extremal in NESS [11, 19], but they have been challenged and later proven wrong [19, 20].

A nice analogy between equilibrium states and NESS can be drawn with electrostatics and magnetostatics, as shown in Table 1.1. In electrostatics all currents vanish by definition and only the charge distribution is of interest. Likewise in equilibrium all currents vanish in favor of DB and only the probability density function (PDF) is of interest. On the other hand in magnetostatics currents are steady and produce in time constant magnetic fields. In the theory of magnetostatics the focus resides on the electric currents and the charge distribution is often neglected, as well as in NESS the probability distribution is not considered [11].

[2] By *net flux* we mean the sum of directed fluxes for a single possible transition, i.e. net flux equals $r_{BA} - r_{AB}$ for transition A $\leftrightarrow$ B (see below).

stationary charges/no fluxes	$\Rightarrow$	electrostatics	$\Leftrightarrow$	equilibrium
steady currents/fluxes	$\Rightarrow$	magnetostatics	$\Leftrightarrow$	NESS

Table 1.1: Analogy between equilibrium and nonequilibrium steady states vs. electrostatics and magnetostatics. The absence of any currents or fluxes in electrostatics can be compared to the *detailed balance* (DB) condition for equilibrium states in statistical physics. Likewise the existence of steady (cyclic) fluxes in NESS can be related to steady current in magnetostatics [11]. Taken and modified from [21].

Chapter 2

Theory

2.1 Introduction

In this chapter we want to review to most important ideas needed to introduce our new approach for a potential of nonequilibrium steady states. The main concepts are *invariant manifolds* from dynamical system theory and evolution equations for probability distributions, such as the Fokker-Planck and Master equation. We will begin with a brief description of dynamical systems in Section 2.2 and proceed further with stochastic processes in Section 2.3.1.

2.2 Dynamical Systems

The study of *dynamical systems* (DS) became very popular among mathematicians or physicists due to their wide range applicability. Dynamical systems can be used to describe for example classical physics, e.g. a pendulum, the flow of water in a river, the amount of mosquitoes swarming around a lake in the summer or weather simulations [22, 23].

The point of interest in dynamical systems is the long-term time evolution. Because dynamical systems often involve non-linearity, complex behavior like periodic orbits or even chaos can be observed. Hence long-term predictions become impossible, e.g. a (nearly exact) weather forecast of one month. The focus of analyzing dynamical systems shifts from finding exact solutions to a more structural or topological analysis of the system. These includes finding fixed points, attractors and repellors, etc., and analyze their stability and dependence on control parameters. The latter is known as bifurcation theory and deals with topological changes in the system due to control parameter [22–24].

In the next section we introduce the basics of dynamical systems theory and will focus mainly on stationary and periodic solutions, namely *fixed points*, *limit*

cycles and *invariant manifolds*. We sometimes restrict ourselves to two-dimensional systems only to reduce complexity.

2.2.1 Basics

A dynamical system is defined by assigning to each possible state a change rate for all times. For example a certain birth-death ratio for every amount of individuals in case of a population dynamical model.

Following [25], a *dynamical system* can be described as an autonomous differential equation, defined on a differentiable manifold $\mathcal{M}$

$$\frac{\mathrm{d}x}{\mathrm{d}t} \equiv \dot{x} = f(x), \tag{2.1}$$

where $x \in \mathcal{M}$ and f is a smooth vector field. For our purposes $\mathcal{M} \subseteq \mathbb{R}^n$ and therefore has a single chart, i.e. our standard Cartesian coordinates [25, 26].

A solution for the system in Eq. (2.1) is a *flowline* or *integral curve* $\varphi(x,t)$ of the *flow* $\varphi_t(x) = \varphi(x,t)$ which satisfies [27]

$$\frac{\mathrm{d}}{\mathrm{d}t}\varphi(x,t) = f\left(\varphi(x,t)\right). \tag{2.2}$$

We say that the vector field f generates the flow φ_t, whose flowrate $\mathrm{d}_t\varphi$ corresponds to f in Eq. (2.1). In other words for any position s the flow $\varphi_t(s)$ follows the vector field $f(\varphi_t(s))$. Given an initial condition $\varphi(x_0, t_0) = x_0 \in \mathcal{M}$, the initial value problem $\gamma(t_0) = x_0$ has an unique solution $\gamma_{x_0}(t)$ called *trajectory* or *orbit*. That is a flowline parameterized in time t [25, 27].

Drawing all flowlines together into the space of $\mathcal{M}$ creates the so-called *phase space*. This drawing is already known from classical mechanics and statistical physics. Figure 2.1 is an example of a two-dimensional phase space called *phase plane*. For autonomous systems a qualitative insight of the system can be gained even if an analytic solution is missing, e.g., the existence of fixed points and closed orbits can be observed [22, 24].

It is important to note here that due to uniqueness of f, the trajectories of f cannot intersect, because if they would, the rate of change at x, $\dot{x} = f(x)$ would not be unique. This is the reasons why the phase space of a dynamical system does not look fuzzy, filled with criss-crossing trajectories, as one sees in Figure 2.1 [22].

2.2.2 Fixed points

Let us focus now on a special kind of solutions with particular physical importance namely the stationary ones, called *fixed points* x^*, *equilibria* or *zeros*. These are defined by

$$\dot{x} = f(x^*) \stackrel{!}{=} 0. \tag{2.3}$$

Once found an equilibrium, we may ask what happens to small perturbations, will they grow or decay? This behavior is analyzed within *stability analysis*. There are

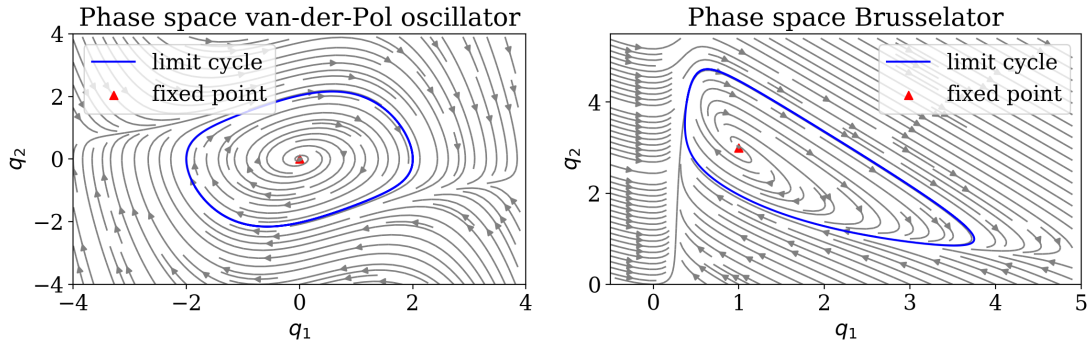

Figure 2.1: Phase space plot of the van-der-Pol oscillator (on the *left*) with $\mu = 0.4$ and Brusselator (on the *right*). Plotted are the unstable equilibria (red dot) enclosed in a stable or attracting limit cycle (blue line). The gray lines are flowlines of the respective system, whose direction is indicated by small arrows. We can observe the attractive behavior of the limit cycles as the flowlines are approaching them. These limit cycles are asymptotically stable and globally attractive since they are the only attractors. *Own simulations.* See Sec. 3.3 and references for further details [24, 25].

different types of stability for equilibria, *stable*, *unstable* and as special case *center*. In case of a stable equilibrium perturbations will decay in time. Therefore the flow is directed towards them, we call them *attractors* or *sinks*. Whereas for unstable equilibrium perturbations will grow over time because the flow points away. They are also called *repellers* or *sinks*.

A special case occurs if perturbations neither grow or decay over time, which needs special treatment. Such equilibrium is known as a *center*. This for example occurs for an ideal pendulum, where solutions are cyclic trajectory around the center fixed point or concentric circles. This introduces another kind of solutions, the *closed* or *periodic orbits*. These will be discussed later in Section 2.2.3.

Speaking of equilibrium we may think about potentials where one analyzes similar quantities, that is equilibrium can be stable, unstable or even meta-stable [22, 23].

A dynamical systems can be in principle be highly nonlinear. To analyze the stability of our system to small perturbations we linearize it, that is, we approximate our system *locally* with the Jacobian matrix $(\mathrm{D}f)_{ij} \equiv \partial_j f_i$ of f. Then the eigenvalues λ_i of the *linearized* system

$$\dot{y} = \mathrm{D}f(x^*)y, \tag{2.4}$$

are considered. This linearization approximates the nonlinear system (2.1) in x^* and is only valid within some neighborhood U of x^*, similar to the local derivative of any function.

Let $\{\lambda_i\}_i$ be the eigenvalues of $\mathrm{D}f(x^*)$. The fixed point x^* is called *hyperbolic* if the real-part $\Re(\lambda_i)$ is non-zero for all eigenvalues. A hyperbolic fixed point is *attracting* if $\Re(\lambda_i) < 0$, $\forall i$, and *repelling* if $\Re(\lambda_i) > 0$, $\forall i$. Furthermore if there are λ_+ and λ_- such that $\Re(\lambda_+) > 0$ and $\Re(\lambda_-) < 0$ x^* is called a *saddle*. A non-hyperbolic fixed point or *center* has purely imaginary eigenvalues and thus created cyclic orbits around x^* [23, 25].

For a hyperbolic equilibrium the Hartman-Grobman theorem ensures the existence of such linearizing mapping as (2.4). This mapping preserves the structure of the flow via mapping the flow φ_t to $e^{\mathrm{D}f(x^*)t}$. This can be chosen even to preserve time parameterization as well [25].

So far we did not consider any dependence of the existence and position of the equilibria on any control parameter of the system. In fact changes of stability, position and existence of equilibria can occur due to changes in control parameters. Changes where these properties of an equilibrium change are called *bifurcation*. We will not deal with bifurcations in the remainder of this thesis.

2.2.3 Periodic solutions

Nonlinear systems possess another type of special solutions, namely *periodic* or *closed orbits*. Any solution trajectory $\gamma(t)$ of Eq. (2.1) which satisfies $\gamma(t+\tau) = \gamma(t)$ for all t is known as periodic solution. τ is the so-called period time. In nonlinear systems this cyclic motion is not limited to orbits around a non-hyperbolic equilibrium. For those system there sometimes exits a limit set.

A *limit set* of x is the set of *limits points* p for which there exists a series $(t_n(x))_{n\in\mathbb{N}}$ such that the distance $|\varphi_{t_n}(x) - p|$ vanishes in the limit $t \to \infty$. The limit set is denoted by $\omega(x)$. An $\alpha(x)$-*limit set* is the set of points for which t goes to negative infinity. A solutions whose limit set is a cyclic orbit is also called a *limit cycle*.

What immediately comes into mind is the question if one can also do a stability analysis for periodic solutions. To answer this we need to introduce the concepts of attracting and repelling closed sets, generalizing the idea from single fixed points.

We define an *attracting* periodic solution γ if within some neighborhood $x \in U$ of γ for each $\epsilon > 0$ and future time the distance $|\varphi_t(x) - \gamma| < \epsilon$. Imagine an ϵ-sized "tube" around γ which contains the flow. Note that with this definition solutions (as in the case of center fixed points) with constant distance to γ are called attracting, but do not approach γ any further as time progresses, for example, the concentric solutions of a harmonic pendulum. It is possible

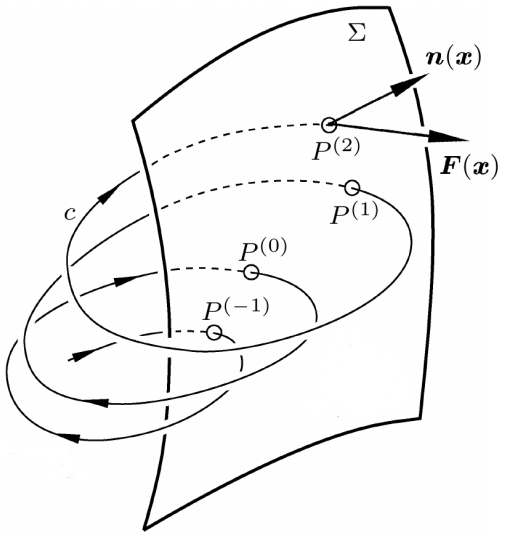

Figure 2.2: Example of a Poincaré cross-section Σ. A flowline c of the dynamical system $F(x)$ intersects with the Poincaré section Σ at points $P^{(k)}$. $n(x)$ is the normalvector of Σ at x. These intersections are equilibria of the so-called Poincaré map, see Eq. (2.5). Taken from [24].

that periodic solutions have fixed radii, hence two solutions can be ϵ-close, but none will end in each other. If furthermore the distance $|\varphi_t(x) - \gamma| \to 0$ as $t \to \infty$, we call it *asymptotically stable*. Solutions which do not fulfill those two stability criteria are called *unstable* [28].

Another way to look at periodic solutions is the *Poincaré map* or *first return map*. For such we define a hypersurface Σ of dimension $n-1$ which is nowhere parallel to the flow. Σ can be of any shape and is not required to be a flat hyperplane. A simplified example is shown in Figure 2.2. The difficulty in selecting Σ is to ensure that intersections only occur after a full period, if the orbit has a winding number greater than one. Σ is also called *Poincaré cross-section*. The Poincaré map P then is

$$\begin{aligned} P :&\Sigma \to \Sigma \\ &s_i \mapsto s_{i+1}, \end{aligned} \tag{2.5}$$

where s_i is the point of the i-th intersection in time and s_{i+1} the next. Here, one already sees the advantage that cyclic solutions are reduced into a set of points. A limit cycle by definition is a fixed orbit and therefore it will produce a single intersection s^* with $P(s^*) = s^*$. Thus s^* is an equilibrium of P.

Let's stay with this result a bit longer. A limit cycle is transformed into a equilibrium by transforming the state space. Abstracting we can say that a nonequilibrium but cyclic solution is mapped via a specific transformation of the phase space into equilibrium. This concept will be an important idea later in the transformation into the so-called *cycle space* [23, 28].

2.2.4 Invariant sets and manifolds

An *invariant set* S for a flow φ_t is defined as

$$\varphi_t(x) \in S,\ \forall x \in S \text{ and } \forall t. \tag{2.6}$$

We call S invariant under the flow φ_t. Furthermore if S is a manifold, it is called an *invariant manifold*. Important examples, the stable and unstable manifolds, will be discussed in Section 2.2.5.

Because stationary behavior is important while studying a dynamical system, a generalization for equilibria and periodic orbits is a *nonwandering set*, a collection of nonwandering points. A point p is called a *nonwandering point* if given any neighborhood U of p, there exists an arbitrary large t such that $\varphi_t(U) \cap U$ is a non-empty set. We can straightforwardly conclude that the flow will forever stay within U.

2.2.5 Stable and unstable manifolds

Looking again at equation (2.4) and defining $A \equiv \mathrm{D}f(x^*)$

$$\dot{y} = Ay, \tag{2.7}$$

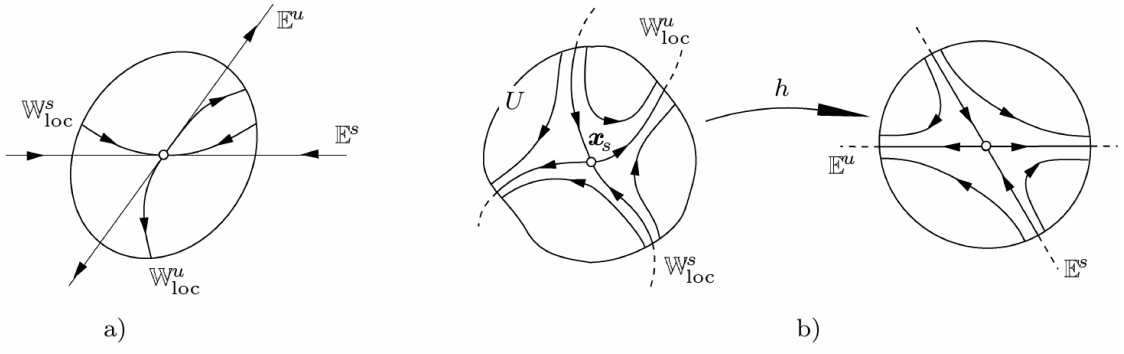

Figure 2.3: Visualization of invariant subspaces and manifolds as well as Hartman-Grobman theorem. Panel (**a**) shows the stable manifold theorem: the local subspaces $\mathbb{E}^s$ and $\mathbb{E}^u$ of the linearized system Eq. (2.4) are tangential to the corresponding invariant manifolds $\mathbb{W}^s$ and $\mathbb{W}^u$ in the hyperbolic equilibrium (indicated by the circle). Pabel (**b**) shows the Hartman-Grobman theorem, which states that there exists within a neighborhood U a linearizing mapping h of the flow φ that is structure and time preserving. This mapping h uniquely maps the invariant manifolds onto the invariant subspaces. Taken from [24].

we obtain a linear ordinary differential equation. The solution of Eq. (2.7) reads

$$y(t) = e^{At} y_0, \tag{2.8}$$

given an initial value y_0. The operator e^{At} defines a flow $\varphi_t(y) = e^{At}y$, as in the Hartman-Grobman theorem.

As before let λ_i be the eigenvalues of A and v_i the corresponding eigenvectors. What happens if an eigenvector serves as initial condition, $y_0 = cv_i, c \in \mathbb{R}$? The answer gives the motivation for an *invariant subspace*

$$\varphi_t(cv_i) = e^{tA} cv_i = ce^{t\lambda_i} v_i \in \text{span}\,(v_i)\,, \forall t. \tag{2.9}$$

The flow stays for all times in a subspace spanned by v_i, the so-called invariant subspace. These are divided into three different kinds,

$$\begin{aligned} \mathbb{E}^s &\equiv \text{span}\,\{v_i \,|\, \Re(\lambda_i) < 0\}\ \textit{stable subspace}, \\ \mathbb{E}^u &\equiv \text{span}\,\{v_i \,|\, \Re(\lambda_i) > 0\}\ \textit{unstable subspace}, \\ \mathbb{E}^c &\equiv \text{span}\,\{v_i \,|\, \Re(\lambda_i) = 0\}\ \textit{center subspace}, \end{aligned} \tag{2.10}$$

with dimensions $\dim(\mathbb{E}^s) = n_s$, $\dim(\mathbb{E}^u) = n_u$, $\dim(\mathbb{E}^c) = n_c$. With n the dimensions of the system this obviously fulfills $n = n_s + n_u + n_c$. A graphical representation of invariant subspaces is given in Figure 2.3.

If we rewrite the last term of Eq. (2.9) by splitting real and imaginary part with $\lambda_i = \Re(\lambda_i) + i\Im(\lambda_i) \equiv \alpha + i\beta$

$$e^{t\lambda_i} v_i = e^{t\alpha} e^{it\beta} v_i, \tag{2.11}$$

one sees that solutions lying in $\mathbb{E}^s$ exponentially decay forwards in time, because $\alpha < 0$, as $t \to \infty$, $e^{t\alpha}$ goes to zero. This decay can be either monotonic, $\beta = 0$, or oscillatory, $\beta \neq 0$. Analogously, solutions in $\mathbb{E}^u$ grow exponentially ($\alpha > 0$) or if in $\mathbb{E}^c$ do neither ($\alpha = 0$). Note that under time reversal a stable equilibrium becomes unstable. Solutions approaching x^* in positive time will go away under $t \mapsto -t$ and vice versa, because we invert direction by time reversal.

These subspaces are as the linearized system (2.4) only valid in some neighborhood U of x^* close to equilibrium. For the nonlinear system an analog is defined with the *local invariant manifolds* $\mathbb{W}$. The definitions state

$$\begin{aligned} \mathbb{W}^s_{loc}(x^*) &= \left\{ x \in U \,\middle|\, \lim_{t\to+\infty} \varphi_t(x) = x^* \text{ and } \varphi_t(x) \in U,\, \forall t \geq 0 \right\} \\ \mathbb{W}^u_{loc}(x^*) &= \left\{ x \in U \,\middle|\, \lim_{t\to-\infty} \varphi_t(x) = x^* \text{ and } \varphi_t(x) \in U,\, \forall t \leq 0 \right\}, \end{aligned} \tag{2.12}$$

where $\mathbb{W}^s_{loc}$ is the *local stable invariant manifold* and $\mathbb{W}^s_{loc}$ the *local unstable invariant manifold* of x^*. Here we see that the concept of stable and unstable is not invariant under time reversal. Thus the stable invariant manifold is the local set of points within U where flow will reach x^* in positive time direction. The unstable invariant manifold is the local set where the flow originated in x^*. Equivalently one can say the flow will reach x^* under time reversal, ergo in negative time direction.

The following *stable manifold theorem for a fixed point* theorem gives existence and important properties of this manifolds,

Theorem 1. *Let x^* be a hyperbolic fixed point of $\dot{x} = f(x)$. Then there exist a local stable and unstable manifold $\mathbb{W}^s_{loc}(x^*)$ and $\mathbb{W}^u_{loc}(x^*)$ which*

(i) have the same dimensions n_s, n_u as the corresponding linear subspaces, and

(ii) are tangential to the corresponding linear subspace in x^* [25].

These concepts can be extended globally as *global invariant manifolds* $\mathbb{W}^s$ and $\mathbb{W}^u$

$$\begin{aligned} \mathbb{W}^s &= \bigcup_{t\leq 0} \varphi_t \left(\mathbb{W}^s_{loc}(x^*) \right) \\ \mathbb{W}^u &= \bigcup_{t\geq 0} \varphi_t \left(\mathbb{W}^u_{loc}(x^*) \right). \end{aligned} \tag{2.13}$$

The global stable invariant manifolds is the union of points in $\mathcal{M}$, whose flow will end up in the local stable invariant manifold. This motivates to call them also *domain of attraction*. Analogously by replacing $t \mapsto -t$ on finds the unstable manifold or *repelling set*. Note that invariant manifolds are unique just as the flow [25].

Due to existence and uniqueness theorem of solutions of (2.1) two stable (or two unstable) invariant manifolds of two distinct equilibria cannot intersect, nor a invariant manifold *cannot intersect* with itself. Nevertheless intersection of stable and unstable invariant manifolds of the same or distinct equilibrium is possible and reflects complex behavior. Intersection of manifolds of the same equilibrium are

called homoclinic and intersection of the manifolds of different equilibria are called heteroclinic [24, 25].

Invariant here means that a set will not change under the flow as time progresses. The invariant subspaces, defined by the linearized system, are approximations of the local invariant manifolds and tangential to them in x^* but both are only valid within some neighborhood of x^*. The invariant manifolds are the nonlinear counterparts [24].

The careful reader may ask two question right now: is there a center manifold and do invariant manifolds have periodic solutions? The answer to the first is yes: there is a concept of *center manifold*. Just to give an idea what they are, the main aspects are reviewed here.

Remember that the center subspace $\mathbb{E}^c$ is spanned by eigenvectors with vanishing eigenvalue. Then there exists a center manifold $\mathbb{W}^c$ tangential to $\mathbb{E}^c$ in x^*. The center manifold in contrast need not be unique [24, 25].

The answer to the second question is also yes: there are invariant manifolds for periodic solutions. These are defined as follows.

$$\begin{aligned} \mathbb{W}^s_{loc}(\gamma) &= \left\{ x \in U \,\middle|\, \lim_{t\to+\infty} |\varphi_t(x) - \gamma| = 0 \text{ and } \varphi_t(x) \in U, \text{ for } t \geq 0 \right\} \\ \mathbb{W}^u_{loc}(\gamma) &= \left\{ x \in U \,\middle|\, \lim_{t\to-\infty} |\varphi_t(x) - \gamma| = 0 \text{ and } \varphi_t(x) \in U, \text{ for } t \leq 0 \right\}, \end{aligned} \tag{2.14}$$

where γ is a periodic solution and U a neighborhood of x^* [25].

2.2.6 A question of dimensions

At this point we could go on with some more complex behavior in nonlinear dynamical systems, such as bifurcations, strange attractors, fractals and chaos. But in two dimensions we have the lucky situation to have the Poincaré-Bendixon theorem. For two dimensional systems this theorem states there are only three possible types of invariant manifolds, namely,

(i) equilibria,

(ii) closed orbits, and

(iii) unions of equilibria and trajectories connecting them.

Such complicated things like strange attractors and chaos[1] cannot occur in two dimensions. This obviously makes our life lots easier.

Another useful theorem for two-dimensional systems is the following.

Theorem 2. *Inside any closed orbit γ there must be at least one equilibrium. If all equilibria inside γ are hyperbolic, then there must be an odd number, $2n+1$, of which n are saddles and $n+1$ either sinks or sources.*

[1] See e.g. [25] or [22] for further reading.

Fokker-Planck and Master-equation	$\Rightarrow$	motion of probability density
Langevin	$\Rightarrow$	noisy motion of single particle

Table 2.1: Different stochastic evolution equations. While Fokker-Planck and Master equations describe dynamics of probability distributions, which are related to ensemble averages, the Langevin equation describes realizations of fluctuating processes, out of which ensemble averages can be obtained by means of simulations.

As a consequence, we can define an axis connecting the inside fixed point with the closed orbit, which will be needed later in the cycle transformation, see Sec. 3.1. This furthermore yields that if we have a limit cycle, which is a closed orbit, we can be sure that there always is a fixed point enclosed.

2.3 Stochastic Dynamics

In real-world systems time evolution often shows irregularity and complexity, which cannot be related to any deterministic evolution law. Such behavior is called fluctuations, and can be caused by complex or unknown internal or external influences called noise. This can be for example a large number of particles interacting, like a particle bouncing around in a fluid, where there is no hope that we can predict all collisions, since we do not know every initial position, or an intrinsically non-deterministic behavior, like in quantum systems.

Fluctuating systems are known as *stochastic systems*. These can be found in numerous fields, e.g. in physics, theoretical biology, and chemistry. Some examples are motion of a Brownian particle, growth of bacterial population, actual arriving times of metros in a station. The methods of stochastic systems can also be applied in economics and in finance. One example is the Black-Scholes theory in finance.

Stochastic systems are described by equations such as Langevin, Master and Fokker-Planck equation, where the first takes noise into account on a microscopic level, the last one refrains from the microscopic picture by describing the evolution of averages.

Due to fluctuations we measure different values for different realizations, i.e., for different initial conditions for the example of the particle in a fluid. In analogy to thermodynamics we introduce the *Gibbs ensemble*. A Gibbs ensemble is defined as a great number of independent system with identical dynamics but with different phase, which is their configuration and velocity [29]. We can define ensemble averages $\langle A \rangle$ of each single measurement A_i [9, 29]

$$\langle A \rangle \equiv \lim_{N \to \infty} \frac{1}{N} \sum_{i=1}^{N} A_i. \tag{2.15}$$

In this section an introduction to stochastic systems is given. We will begin with basic concepts like stochastic processes and Markov chains. From the Chapman-

Kolmogorov equation for transition probabilities we will go on to the Langevin equation and stochastic calculus. Finally we will introduce concepts for evolution of probability density functions, i.e. Fokker-Plank and Master equation, in contrast to the stochastic calculus.

2.3.1 Stochastic Processes

A *random variable* X is a (observable) quantity, whose instantaneous realization cannot be predicted, e.g. the number shown by a thrown die. A *stochastic process* is a process depending on a random variable, i.e. $Y_X(t) = F(X,t)$ where Y_X is a stochastic process as an arbitrary function F of a random variable and time t. t does not need to be interpreted as time but in the context of physics it is often. Such a process is described in the ensemble picture. Substitution of X with the value of one specific realization x gives back the classical physical formulas.

Given a continuous probability distribution $p_X(x)$, also called probability density, averages can be calculated from

$$\langle Y_X(t)\rangle = \int_\Omega F(x,t)p_X(x)\mathrm{d}x, \tag{2.16}$$

where Ω is the sample space, i.e., the set of all possible states. If Ω is discrete averages can be calculated as summation $\langle Y_X(t)\rangle = \sum_k F(x_k,t)p_k$.

Of special use are the so-called *moments* μ_n

$$\mu_n = \langle x^n\rangle = \int x^n p(x)\mathrm{d}x, \tag{2.17}$$

which we will see later in the Kramer-Moyal expansion.

One important probability distribution is the *Gaussian distribution* or *normal distribution*. Given the first two moments, average μ and variance σ^2 it is given by

$$p(x) = \frac{1}{\sqrt{2\pi\sigma^2}}\exp\left(-\frac{(x-\mu)^2}{2\sigma^2}\right). \tag{2.18}$$

Two examples of the Gaussian distribution are shown in Figure 2.4.

We are interested in the time evolution of a system and therefore consider a stochastic process as a sequence of random variables $\{X_{t_i}\}_i$ indexed by a parameter t_i, which is often used as time. We assume $t_1 < t_2 < \ldots < t_n$ with finite n. Keep in mind that t can be a continuous variable. A realization x_i of each X_{t_i} for all t_i's is called a *trajectory*

$$\{x_1,t_1;x_2,t_2;\ldots;x_n,t_n\}. \tag{2.19}$$

The *joint probability* expresses the likelihood to observe a trajectory

$$p_n(x_1,t_1;\ldots;x_n,t_n). \tag{2.20}$$

The index of p_n here emphasizes that n points are given by a fixed value. If less $k < n$ points are given, the probability to find these subset of a trajectory

$$p_k(x_1, t_1; \ldots; x_k, t_k) = \int p_n(x_1, t_1; \ldots; x_n, t_n) \mathrm{d}x_{k+1} \cdots \mathrm{d}x_n, \tag{2.21}$$

is the so-called *marginal distribution* p_k. The marginal distribution is given by the integration over the remaining $x_{k+1} \ldots x_n$ state variables.

If we prescribe $x_1, \ldots, x_k$ with fixed values or conditions, we can determine the joint probability of the other $n - k$ variables, which is the so-called *conditional probability*

$$p_{n-k}(x_{k+1}, t_{k+1} \ldots; x_n, t_n | x_1, t_1; \ldots; x_k, t_k). \tag{2.22}$$

This is the conditional probability of $X_{k+1}, \ldots, X_n$ conditional that $X_1, \ldots, X_k$ have the values $x_1, \ldots, x_k$. We interpret this as *transition probability* of a system to evolve into $x_{k+1}, \ldots, x_n$ given that the remaining state variables have fixed values. Bayes rule gives the connection between conditional and marginal probability [16]

$$p_{n-k}(x_{k+1}, t_{k+1}; \ldots; x_n, t_n | x_1, t_1; \ldots; x_k, t_k) = \frac{p_n(x_1, t_1; \ldots; x_n, t_n)}{p_k(x_1, t_1; \ldots; x_k, t_k)}. \tag{2.23}$$

2.3.1.1 Markov property

Many physical processes are independent of their evolution history but solely depend on the current state, i.e., the future (x_{i+1}, t_{i+1}) only depends on the current (x_i, t_i) state. This is known as *Markov property* or sometimes referred as *memoryless* processes. The transition probability is hence given by two-point functions $p_2(x_{i+1}, t_{i+1} | x_i, t_i)$[2]. The time evolution is fully determined by p_2, and therefore it is called a *propagator*. If the propagator is furthermore time independent, it is called *stationary* or *homogeneous* Markov process. One example of such process is Brownian motion.

The Markov property enables to use some handy simplification when treating such stochastic processes. For a full description of the system we only need two functions, namely $p_1(x, t)$, the probability density, and a propagator $p_2(x', t' | x, t)$. Any joint probability p_n can be reduced to

$$p_n(x_1, t_1; \ldots; x_n, t_n) = \left[\prod_{i=1}^{n-1} p_2(x_{i+1}, t_{i+1} | x_i, t_i) \right] p_1(x_1, t_1). \tag{2.24}$$

Let's set $k = 2$ for readability. Integrating Eq. (2.24) over x_2 we find the marginal distribution $p_2(x_3, t_3; x_1, t_1)$. Using Bayes rule $p_2(x_3, t_3; x_1, t_1) = p_2(x_3, t_3 | x_1, t_1) \cdot p_1(x_1, t_1)$ and dividing both sides by p_1 we find an important equation of this section: the Chapman-Kolmogorov equation (CKE)

$$p_2(x_3, t_3 | x_1, t_1) = \int p_2(x_3, t_3 | x_2, t_2) p_2(x_2, t_2 | x_1, t_1) \mathrm{d}x_2. \tag{2.25}$$

[2]This is read from right to left, i.e., the system evolves $(x', t') \leftarrow (x, t)$

Because the whole dynamics for a Markov process are encoded in p_1 and p_2, we can rewrite the CKE (2.25) as

$$p_1(x_3, t_3) = \int p_2(x_3, t_3|x_2, t_2)p_1(x_2, t_2)\mathrm{d}x_2, \tag{2.26}$$

which is the second form of the CKE. We will call the (2.25) *two-point CKE* and the latter *one-point CKE*.

An often studied version of a Markov process is a *Markov chain*. It has a discrete sample space. If furthermore the sample space has finite N elements, we call it a *finite Markov chain*. The transition probability between all states then can be represented as a $N \times N$ matrix T_t, where t denotes time. T is a so-called *stochastic matrix*, which has non-negative entries (since probabilities cannot be negative) and each column sums up to unity. In this matrix representation p_1 takes the form of a $N \times 1$ vector. The time evolution for a stationary Markov chain can be expressed by $p_1(t') = T_\tau p_1(t)$, where $\tau = t' - t$. Stationary distributions $p_1^* = \lim_{t\to\infty} T_t p_1(t_0)$ are eigenvectors of T with unity eigenvalue, $p^* = Tp^*$.

The concept of a Markov process, which is by definition independent from history, can be used to model a process with finite memory m by introducing additional m variables. Such a process is called higher order Markov process or Markov process with memory m. Hence we call it *m-th* order Markov process. For example we can rewrite a process depending on the last two states in history as a second order Markov process by adding one variable, which takes the second last as a new state vector with one more dimension [16].

2.3.2 Langevin equation and stochastic differential equations

Real-world physics often includes fluctuations, since we cannot control all parameters. Whether fluctuations (and thus a stochastic approach) are negligible is a question of scales. Consider for example a particle with mass m in a fluid at temperature T. From the equipartition theorem (in one dimension, for simplicity) $\frac{m}{2}\langle v^2\rangle = \frac{k}{2}T$, with k Boltzmann constant and v velocity, it follows that the thermal velocity $v_T \propto \sqrt{m^{-1}}$. Hence for small m the stochastic character is not negligible. The particle will collide with the molecule of the fluid in a random fashion and so the velocity jumps at each collision. This is known as *Brownian motion*.

To take these fluctuations into account we need to modify the corresponding *macroscopic* deterministic force relation by introducing a new additive force: a Langevin force. Hence the force acting on a particle becomes a stochastic quantity and with that also the velocity [9]. The Langevin equation (LE) for Brownian motion reads

$$\dot{v} = \underbrace{-\gamma v}_{\text{deterministic}} + \underbrace{\sigma\Gamma(t)}_{\text{stochastic}} . \tag{2.27}$$

$\Gamma(t)$ is a Langevin force and σ a scaling constant. See Figure 2.4 for some typical trajectories and the corresponding probability distribution.

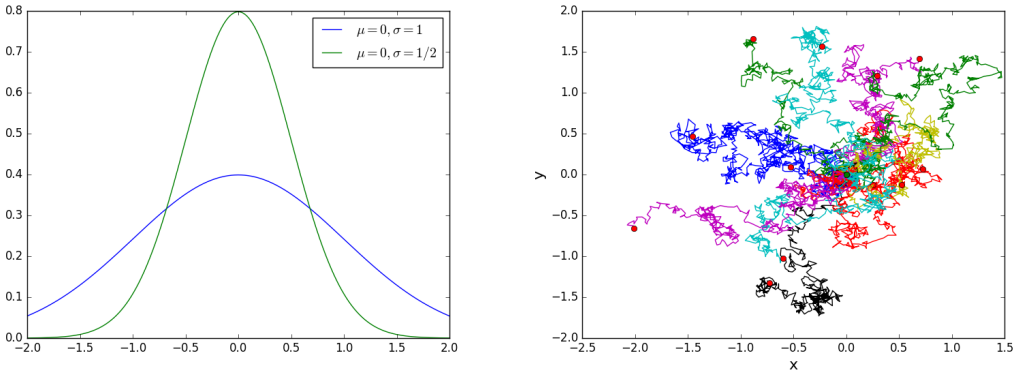

Figure 2.4: *Left* panel shows Gaussian distributions [see Eq. (2.18)]. Plotted distributions have different standard deviations σ and same mean value $\mu = 0$. *Right* panel shows 12 example trajectories of two-dimensional Brownian motion. The plotted Brownian motion is purely stochastic $\dot{x} = \sigma\Gamma(t)$ [see Eq. (2.27)]. All trajectories originated in the origin (green dot) and the final position after 500 steps is depicted by the red dot. x and y are in arbitrary units. Γ is a Gaussian distribution as shown in the left panel. *Own simulations.*

The Langevin equation consists of a deterministic and stochastic part. We often know the first part a priori and can define a Langevin equation with the following algorithm.

(i) Write a deterministic macroscopic equation;

(ii) add a stochastic part as Langevin force;

(iii) adjust the coupling constant σ so that your model fulfills expectations.

In [16] this is called a *Langevin approach*. And its the most simple stochastic model one can think of.

Since Eq. (2.27) is a stochastic equation, its properties can only be given within the ensemble picture. On average we expect our deterministic dynamics to hold again and hence it is reasonable to require [9]

$$\langle \Gamma(t) \rangle = 0. \tag{2.28}$$

Multiplying Γ at two different times t and t' gives us the correlation; we assume that the collisions are statistically independent and hence set

$$\langle \Gamma(t)\Gamma(t') \rangle = \delta(t - t'). \tag{2.29}$$

Such a δ-correlated noise source is known as *white noise*, due to its spectrum. Non-δ-correlated noise sources are called *colored noise*.

White noise has a handy implication: δ-correlated Langevin forces are Markov processes. This is caused by the fact that δ-correlation reflects statically independence. Thus, for Brownian motion, the velocity after a collision only depends on the

instantaneous value and not on its history. As mentioned in Sec. 2.3.1.1 we can still model finite memory processes with higher order Markov processes. Often, values for Γ are drawn from a Gaussian distribution similar to Eq. (2.18). The noise then is called *Gaussian white noise*.

The Langevin equation (2.27) is linear. But Langevin equations in general can be non-linear. We write them as

$$\frac{\mathrm{d}X(t)}{\mathrm{d}t} = a(X,t) + b(X,t)\Gamma(t), \tag{2.30}$$

where X is an arbitrary observable. Equation (2.30) is a general *stochastic differential equation* (SDE). SDE's differ from ordinary differential equations, because for example Brownian motion is nowhere differentiable and so the corresponding SDE also is not differentiable. Integration is still possible but there is an additional degree of freedom which led to different interpretations. Widely known are Stratanovich and Itô, which are different choices for how noise is taken into account in a Riemann integral. For further details see references [9, 30].

In Eq. (2.30) we see that b can depend on the random variable X. In case b is constant in X we call it a Langevin equation with *additive noise*. If $b = b(X,t)$ it is called *multiplicative noise*. If a and b are both time-independent and non-zero b multiplicative noise can always be transformed into additive [9].

Let me give some remarks on a Langevin approach. It can be utilized to study stochastic influences on a system whose macroscopic behavior is already known. As in Eq. (2.30) we just add an external force, the Langevin force. This can be applied to dynamical system as of Section 2.2. This leads to the seconds remark: the Langevin approach does not work for internal noise [16]. *Internal or intrinsic noise* cannot be switched off and is inseparably coupled with the mechanism of evolution, and thus a standalone $a(X,t)$ is inaccessible. Examples are chemical reactions and light absorption and emission [16].

2.3.3 Fokker-Planck equation

Instead of adding a stochastic character to known dynamics, as discussed for the Langevin approach in Section 2.3.2, we can view a stochastic process from a different perspective. Consider a homogeneous heat equation in one dimension $\partial_t u = D_t \partial_x^2 u$ with thermal diffusion constant D_t. A solution $u(x,t)$ determines the *deterministic* distribution of heat. The diffusion process itself is, indeed, stochastic but the evolution of the distribution is deterministic. The reason is that diffusion is related to the mean-squared displacement $\langle (x(t') - x(t))^2 \rangle$ where fluctuation are "averaged out". In the same manner the Fokker-Planck equation (FPE) describes evolution of (probability) distributions[3]. Hence the FPE is a deterministic (partial) differential equation for a distribution function of a fluctuating process. The FPE is best suited to deal with a continuous state space. For discrete ones we will use the Master equation in Section 2.3.4.

[3]The heat equation and FPE are mathematically equivalent, if we set the drift-term of the FPE to zero.

We could also solve the Langevin equation and obtain expectation values, but in case of non-linear Langevin equations this could be challenging [9]. Therefore we use the Fokker-Plank equation.

A general form of the Fokker-Plank equation in one dimension is

$$\frac{\partial p}{\partial t}(x,t) = \left[-\frac{\partial}{\partial x}\mathcal{K}(x,t) + \frac{\partial^2}{\partial x^2}\mathcal{D}(x,t)\right] p(x,t), \tag{2.31}$$

with $\mathcal{K}$ drift and $\mathcal{D}$ diffusion coefficients. These coefficients can depend on position x and time t, as indicated, and therefore the partial derivatives on the right-hand side also apply to them. In higher dimensions $\mathcal{K}$ becomes a drift vector and $\mathcal{D}$ a diffusion tensor, see Eq. (A.1).

2.3.3.1 Kramers-Moyal expansion

We aim here to derive a differential expression for the probability distribution p, which is the Fokker-Planck equation. We follow the derivation in [9]. Beginning with the Chapman-Kolmogorov equation (2.26) we transform it into an expression of moments. Afterwards the moments are recast into the so-called Kramer-Moyal expansion coefficients, which is a series expansion. If this series stops after the second term we arrive at the Fokker-Planck equation.

Consider the the identity

$$p_2(x', t+\tau|x,t) = \int \delta(y-x')p_2(y,t+\tau|x,t)\mathrm{d}y. \tag{2.32}$$

The δ-distribution can be expanded into a Taylor series which yields

$$p_2(x', t+\tau|x,t) = \sum_{\nu=0}^{\infty} \frac{1}{\nu!}\int (y-x)^\nu p_2(y,t+\tau|x,t)\mathrm{d}y \left(\frac{\mathrm{d}}{\mathrm{d}x}\right)^\nu \delta(x-x'). \tag{2.33}$$

We assume that we know all moments μ_ν. By using the definition of moments μ_ν (2.17) and inserting (2.33) into (2.32) yields

$$\frac{\partial p}{\partial t}(x,t) = \left[\sum_{\nu=1}^{\infty}\left(-\frac{\partial}{\partial x}\right)^\nu D^{(\nu)}(x,t)\right] p(x,t), \tag{2.34}$$

known as Kramer-Moyal expansion[4]. The coefficients $D^{(\nu)}$ are called Kramer-Moyal coefficients. We consider here Markov processes; for non-Markovian processes the $D^{(\nu)}$ would depend on earlier times and hence is not so easy treatable.

As a consequence, a Langevin equation with continuous stochastic variable and δ-correlated noise leads to a FPE; the Kramer-Moyal expansion may stop after the second term, see also Section 2.3.3.2. See Appendix A.1.2 for how to obtain drift- and diffusion constant if we know the Langevin equation.

[4]More precisely this is a Kramer-Moyal *forward* (in time) expansion, but it can be shown that forward and backward expansions are equivalent [9].

2.3.3.2 Pawula theorem

The similarity between Eq. (2.31) and (2.34) is evident. We can identify the drift coefficient $\mathcal{K} = D^{(1)}$ and diffusion $\mathcal{D} = D^{(2)}$. But the series in Eq. (2.34) is infinite. The Pawula theorem tells us that an expansion of the distribution function, e.g., the Kramer-Moyal expansion, stops after the first or second term or has infinitely many terms. If it stops at the second one, we find the Fokker-Planck equation, which happens for δ-correlated noise and a continuous state space x. For discrete state spaces the series has infinitely many terms, but we can truncate it after the second term and get an approximate Fokker-Planck equation. Truncating the series at higher order term would lead to negative probabilities but also to a better agreement with the original equation [9].

2.3.4 Master equation

If the state space is discrete, for example in chemical reactions, we are better suited with the Master equation than the Fokker-Planck equation.

The Master equation is an equivalent form of the Chapman-Kolmogorov equation in case of a Markov process. It is a differential equation for the transition probability in the limit of vanishing time difference. This can be rewritten as a differential equation for the distribution function, similar as the Fokker-Planck equation, and reads

$$\frac{\partial p}{\partial t}(x,t) = \int \left[w(x|x')p(x',t) - w(x'|x)p(x,t)\right] \mathrm{d}x', \tag{2.35}$$

with $w(y|x)$ the *transitions per unit time* going from x to y[5]. For a discrete state space, where then *jumps* between the states occur, the Master equation is more compactly written as

$$\frac{\partial p_n}{\partial t}(t) = \sum_{m \neq n} \left[w_{nm}p_m(t) - w_{mn}p_n(t)\right], \tag{2.36}$$

where summation is over the whole state space. w_{nm} is identified as the discrete version of w in case of a transition from m to n, where n and m are discrete indexing parameters. Similarly, p_n is the probability function for the state n. Equation (2.36) can be written in form of a stochastic matrix similar to the ones for Markov processes in Section 2.3.1.1. For further reading also refer for example to [16] or [11]. Furthermore network theoretical approaches are possible for these matrix representation. See [19] for further reading.

The Master equation has an intuitive (physical) interpretation: it is a direct representation of transitions per unit time between all states of a system. Multiply the transition rates w with the probability of a state and we find the actual probability flux j within our systems

$$j_{nm} \equiv \underbrace{w_{nm}p_m}_{\text{influx } n \leftarrow m} - \underbrace{w_{mn}p_n}_{\text{outflux } n \rightarrow m}. \tag{2.37}$$

[5] We have dropped out time dependence in w because for simplicity we assume a stationary stochastic processes.

In the same manner Eq. (2.36) can be reformulated as

$$\partial_t p_n = j_n^{\text{tot}} \equiv j_n^{\text{in}} - j_n^{\text{out}} \equiv \left(\sum_{m \neq n} w_{nm} p_m \right) - \left(\sum_{m \neq n} w_{mn} p_n \right), \tag{2.38}$$

where j_n^{in} and j_n^{out} are the total fluxes entering and leaving state n. Or as conservation equation [11]

$$\partial_t p_n = \sum_{m \neq n} j_{nm}. \tag{2.39}$$

2.3.4.1 Steady state and detailed balance

We now want to focus on stationary states within the network representation of the Master equation. Stationarity entails $\partial_t p_n = 0$ and hence with Eq. (2.36) follows

$$0 = \sum_{m \neq n} \left[w_{nm} p_m(t) - w_{mn} p_n(t) \right] \equiv j_n^{\text{tot}}, \ \forall n, \tag{2.40}$$

where j_n^{tot} is the total flux of n. This can be achieved in two possible configurations: *locally*, where each transition vanishes, or *globally*, where only the total current vanishes.

First we consider the local stationarity, which is given by the *detailed balance* (DB) condition. Detailed balance requires that each possible transition is balanced by its reverse $j_n = 0$, $\forall n$, which is only possible for

$$w_{nm} p_m = w_{mn} p_n. \tag{2.41}$$

Detailed-balanced stationary states are unique and correspond to thermal equilibrium [11]. As we worked out in Section 1.1, for the DB case we can define a thermodynamic-like potential Φ. Considering an arbitrary path $\mathcal{P} = s_i \to s_j \to \ldots \to s_k \to s_l$ trough our system and its reverse, i.e., in opposite direction, $\mathcal{P}^{-1}$ and applying Eq. (2.41) iteratively to each neighboring states, yields

$$p_k = p_i \frac{w_{ji} \ldots w_{lk}}{w_{kl} \ldots w_{ij}} \equiv p_i \frac{\Pi[\mathcal{P}]}{\Pi[\mathcal{P}^{-1}]}, \tag{2.42}$$

where $\Pi[\mathcal{P}] \equiv w_{ji} \ldots w_{lk}$ is the product of transitions rates for path $\mathcal{P}$. Since in equilibrium DB condition holds, Eq. (2.42) is valid for *any* path $\mathcal{P}$ connecting s_i with s_k. This can be called a path independence or integrability condition. Thus we can define a potential Φ_{io} between s_i and an arbitrary reference state s_o from Eq. (2.42) as [11]

$$\Phi_{io} \equiv \ln \left[\frac{\Pi(\mathcal{P})}{\Pi(\mathcal{P}^{-1})} \right]. \tag{2.43}$$

The steady state probability p_i of state s_i can now be written with the potential as [11]

$$p_i \propto \exp\left[\Phi_{io}\right], \tag{2.44}$$

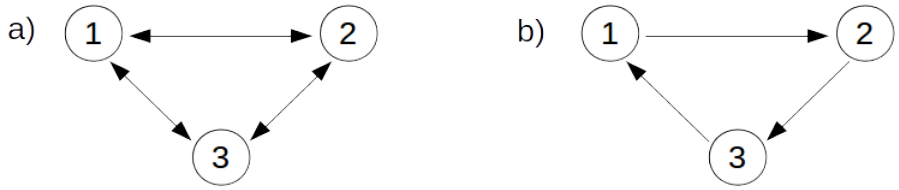

Figure 2.5: Difference of stationary states in a discrete three-state stochastic system. Panel (**a**) shows the *detailed balance* condition where each single transition is balanced by its reverse and hence all net fluxes between each state vanish, see Eq. (2.41). Panel (**b**) shows a *cyclic flux*. Fluxes occur as nonequilibrium steady-state (NESS) where only the sum of all incoming and outgoing fluxes of a state vanishes, see Eq. (2.40).

where proportionality is due to normalization of p. This can also be written as $p_i \propto \exp[-\Phi_{oi}]$ by using logarithmic laws. That form is more alike to the known thermodynamic potential $\exp[-\beta\mathcal{H}]$ as discussed in Sec. 1.1.

For global stationarity there is a set of states where in-between non-zero net fluxes occur. Hence only $j_n^{\text{tot}} = 0$ remains valid. This corresponds to nonequilibrium steady states (NESS), where DB is breached. Hence a potential as in the case where DB holds, Eq. (2.43), is not possible. Since Eq. (2.40) needs to be satisfied, fluxes in the stationary state, if non balanced locally, need to occur in cycles. If they were not in cycles, which means recurrent, the probability would change over time and that contradicts the stationarity. The simplest example is a three state system, $n \in \{1, 2, 3\}$, where

$$j_{21} = j_{32} = j_{31} = \text{const.} \neq 0 \tag{2.45}$$

and all other j's vanish. See Figure 2.5 for a graphical representation of the difference of detailed balance condition and cyclic fluxes.

However, for NESS there exist graph-theoretical approaches to obtain the steady state distribution. Those are based on Kirchhoff's law, which originally was used to describe electrical networks, and consist of decomposing cycles into spanning trees [1,11,19]. While still possible to obtain a steady state distribution, it requires a lot more effort and even NESS are not unique. There are possibly numerous steady states that a system can reach but only one, if any, equilibrium state. Another question currently addressed in nonequilibrium research is what initial conditions lead to the same NESS, that is, determining the so-called *dynamical equivalence class* (see Ref. [11]).

Chapter 3

Methods and concepts

In this chapter we describe our approach towards a nonequilibrium steady state (NESS) potential. For further reading on this ansatz please refer to [1, 7] and [31].

3.1 Cycle transformation

In this section we will get to know the keystone of our approach towards a NESS potential, namely, the *cycle transformation*. The aim of the cycle transformation is to regain detailed balance for NESS and ultimately be able to define a potential. As we know, due to conservation laws, fluxes in NESS can only be closed, cyclic trajectories. The cycle transformation can be seen analogously to the Poincaré cross-section as introduced in Sec. 2.2.3. The $P^{(i)}$'s take the role of new descriptors as replacement for states in a Master equation. Analogously we will recast the states and transitions into a (complete) set of cycles and weights.

Following [1], we (at least for now) assume the our dynamical systems can be described as a Markov process in a finite space. Furthermore, we assume ergodicity, which means that any state can be reached from another in finite time. It ensures the existence of a steady-state [1]. We define a cycle as an ordered set of vertices which form a self-avoiding closed path. The equivalence is the cyclic permutation.

The stationary dynamics can be represented as graph $G = (V, E)$ with N vertices $v_i \in V$ and edges $(i, j) \in E$. The vertices take the role of the process' states and the edges the transitions. The dynamics of the process are encoded in transitions rates w and fluxes j as described in Sec. 2.3.4.

The *cycle transformation* is a decomposition of a graph G into a superposition of cycles with a weight assigned to each cycle. It replaces the vertices V by a set of cycles $\mathcal{C}$ and new edges $E_{\mathcal{C}}$. That defines a new, transformed graph $H = (\mathcal{C}, E_{\mathcal{C}})$. Basically we changed the domain V to $\mathcal{C}$, i.e., states to cycles. Figure 3.1 shows a decomposition of a six state network on the l.h.s. into two possible superpositions

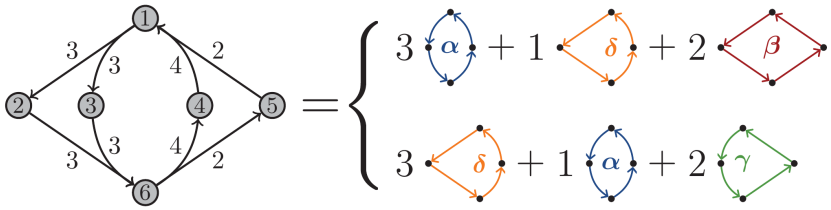

Figure 3.1: Decomposition of a six state network (l.h.s.) into two possible superpositions of cyclic fluxes (r.h.s). The numbers represent the strength of the directed fluxes. Taken from [1].

of cycles[1] on the r.h.s. As we see decompositions are numerous and non-unique but it has been shown that all cycle weights can be chosen non-negative [1].

H gives rise to a new Master equation where the original states and probabilities are replaced by cycles $\alpha \in \mathcal{C}$ and weights or currents c_α. It reads

$$\frac{\mathrm{d}c_\alpha}{\mathrm{d}t} = \sum_{\beta \in \mathcal{C}} v_{\alpha\beta} c_\beta - v_{\beta\alpha} c_\alpha, \tag{3.1}$$

with $v_{\alpha\beta}$ the transition rate from cycle β to α, which replace the transition probabilities w_{ij}. Transitions between cycles take place at states belonging to both cycles. This is expressed with the help of indicator (or passage) functions χ_i^α, which is $\chi_i^\alpha = 1$ if state i lies on cycle α and otherwise zero. The product of indicator functions gives us the common states since it vanishes for non-mutual states. Hence, the transition rate $v_{\alpha\beta}$ is given by [31]

$$v_{\alpha\beta} = \sum_{i \in V} \frac{\chi_i^\alpha \chi_i^\beta c_\alpha^*}{\sum_{\gamma \in \mathcal{C}} \chi_i^\gamma c_\gamma^*}, \tag{3.2}$$

with c^* the steady state weights. It has been recently shown [1] that Eq. (3.1) fulfills detailed balance. Thus, we can write down a potential Φ in the same manner as in Sec. 2.3.4.1, especially Eq. (2.44),

$$c_\alpha^* \propto e^{-\Phi_\alpha}. \tag{3.3}$$

Furthermore, this implies a *path independence* and such can be checked numerically. An example of cycle space (depicted by the circles) is shown in Fig. 3.2 together with two paths connecting the same cycles. One chooses different paths through the cycle space and compare the potential values Φ. Such numerical tests of a candidate ansatz for a NESS potential is the main objective of this thesis. We will elaborate in the following the steps we took to reach this goal.

[1] We label the cycles by Greek letters.

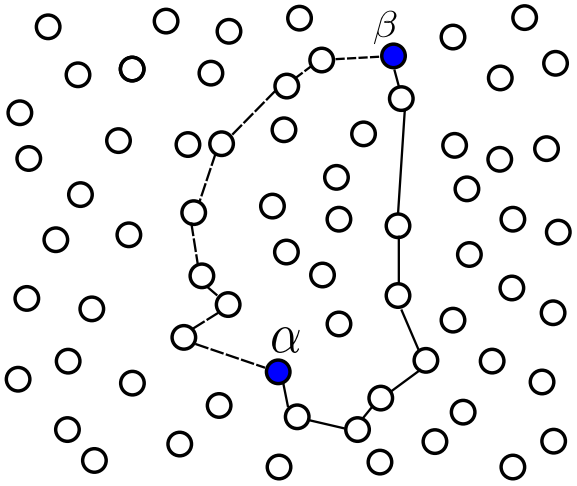

Figure 3.2: A schematic representation of the so-called cycle space. Each circle corresponds to a cycle. Two different paths (solid and dashed lines) connecting the cycles α and β are shown. Detailed balance enables us to multiply transition rate along different path to gain a potential difference independent of the path chosen.

3.1.1 Continuous cycle space

The most important problem at the very core of our approach is the following: to calculate the cycle transition rates v, i.e., evaluate Eq. (3.2), we need to know the steady state weights c^*. This requires a full mathematical solution of the original Master equation. It is argued [31] that this issue can be resolved by using a continuum representation of the problem, i.e., the cycle space, and use the Fokker-Planck equation to find an alternative way to determine the transitions rates v.

A Fokker-Planck equation can be derived from the continuity equation $\partial_t P = \nabla \cdot J$ for the probability density P and current J. In analogy to convection-diffusion processes, the current can be written as the sum of advection or drift current J_K and diffusion current J_D

$$\partial_t P = \nabla \cdot J = \nabla \cdot (J_K + J_D). \tag{3.4}$$

Those currents can be written as

$$J_K = P \cdot \mathcal{K}, \tag{3.5}$$
$$J_D = -\mathcal{D}\nabla P, \tag{3.6}$$

where $\mathcal{K}$ is the drift coefficient or field and $\mathcal{D}$ the diffusion coefficient. As a result, we can differentiate between currents, which arises from drift, J_K, and those which are caused by a diffusion process, J_D. Inserting the above relation into Eq. (3.4) yields a Fokker-Plank equation, same as Eq. (A.1),

$$\partial_t P = \nabla \cdot (\mathcal{K}P - \mathcal{D}\nabla P). \tag{3.7}$$

As we see from Eq. (3.7), we derived a decoupling of the current in drift and diffusion currents. The drift current arises from a deterministic drift $\mathcal{K}$ and diffusion

from a stochastic diffusion process. The drift current is treated as dynamical system, denoted by DS($\mathcal{K}$),

$$\partial_t \varphi = \mathcal{K}(\varphi), \tag{3.8}$$

where φ is the order parameter of the continuum representation. The stationary behavior as the long time limit is dominated by invariant manifolds, i.e., ω-limit cycles and fixed points. Almost all[2] initial conditions will end up after sufficient long time in a stable invariant manifold. As consequence, stable invariant manifolds are the states, which are most likely occupied and hence correspond to maxima in the probability density.

We now devise the following strategy: if we fill the space between the invariant manifolds with a family of non-overlapping, smooth cycles containing the invariant manifolds, we have effectively performed a cycle transformation. See Fig. 3.3 where some members of a cycle family (dashed lines) between the invariant manifolds (solid lines) and a fixed point are shown. The shape of the cycles determines which states in phase space it passes through. If we alter the shape, we alter the states included in the cycle and thus we select different cycles. Those correspond to different states in the cycle space. Hence, if we fix the start and end points of a path in the cycle space, e.g., to be the invariant manifolds, we can define different paths between the manifolds by defining cycle families of different shape.

Distinct cycles are identified by a continuous parameter p onto an axis intersecting the manifolds. An example is also shown in Fig. 3.3. This $\hat{p}$-axis[3] is defined in analogy to the Poincaré cross-section to be nowhere parallel to the flow and uniquely, i.e. only once, intersect each cycle. It is the starting and ending point for each cycle. Within one family the label p replaces the Greek letters for different cycles. As a result, limit cycles then correspond to a *single* state in the cycle space, which is the cycle identified with p and hence have lost the periodic behavior. Furthermore by exploiting detailed balance and integrating transition rates of neighboring cycles between invariant manifolds we arrive at a NESS potential. Since the stable invariant manifolds are most likely occupied they correspond to a minimum in the potential. An explicit formulation how to obtain such a potential will be given in Sec. 3.2.

3.1.2 The Crosswind Operator

In the previous section we filled the space between invariant manifolds with a family of non-overlapping cycles, or strictly speaking, we performed a cycle transformation. Now we want to focus on how the deformation of the trajectories of DS($\mathcal{K}$) into closed orbits is carried-out. We describe the deformation operation with a so-called *crosswind operator* $\mathcal{R}$. This crosswind operator is a local operator, which redirects the flow to be tangential to the closest cycle in the family. This can be imagined as a local crosswind changing the direction of the flow and forcing it into closed orbits.

[2]Indeed, this strongly depends on the topology of the dynamical system and hence the basin of attraction.

[3]We denote by $\hat{p}$ the unit vector of the axis and by the p the intersection value of a cycle with $\hat{p}$-axis.

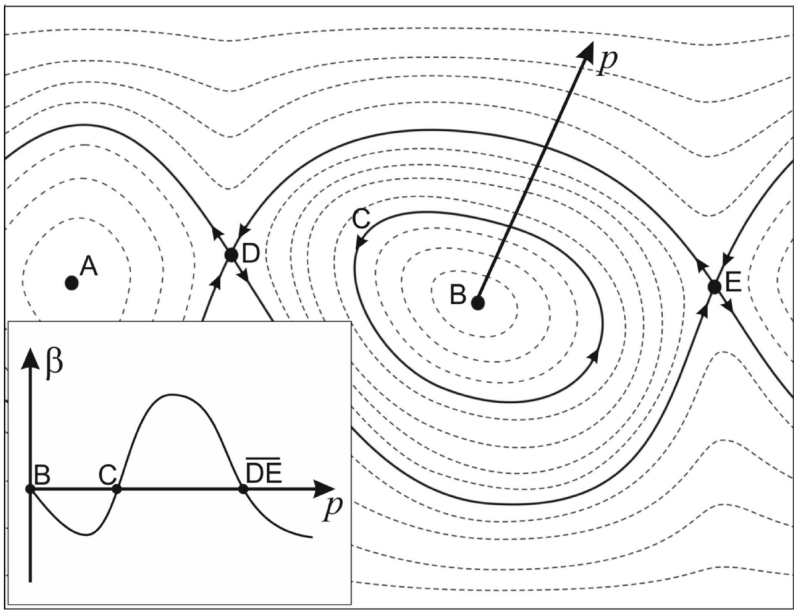

Figure 3.3: Example for a constructed $\mathcal{L}$-drift field. The solid lines represent invariant manifolds. Let us assume that the fixed point B is unstable, C is a stable limit cycle (attractor), and the seperatrix between D and E is unstable. A $\hat{p}$-axis that parameterizes a connection of the manifolds is depicted as well. The inset shows what one expects for a constant crosswind operator, as discussed in Sec. 4.2.1. The closing angle should vanish on the invariant manifolds, since the drift points along these manifolds and hence no crosswind is needed to close these. Taken from [31].

It obviously depends on the cycle family $\mathcal{C}$, i.e., the shape of the cycles. We will usually drop the family dependence and simply write $\mathcal{R}$ but we should keep in mind that $\mathcal{R}$ varies for different families. The application of the crosswind operator on DS($\mathcal{K}$) defines a new dynamical system, which we call DS($\mathcal{L}$),

$$\mathcal{L}(\varphi) \equiv \mathcal{R}(\varphi)\mathcal{K}(\varphi). \tag{3.9}$$

It is argued [31] that there is always a finite diffusivity involved, i.e., $\mathcal{D} > 0$, and hence *both* $\mathcal{K}$ and $\mathcal{L}$ are *possible* trajectories of an ensemble described by a corresponding Fokker-Plank equation. Due to noise influences it is possible that some systems actually are on the trajectories defined by DS($\mathcal{L}$). In other words, one can find systems in the ensemble that follow the cycle defined by DS($\mathcal{L}$) when interpreted as dynamical system.

Let us assume we have a two-dimensional system. The crosswind operator can then be given as rotation matrix[4]

$$\mathcal{R}(\varphi) = \begin{pmatrix} \cos\beta(\varphi) & \sin\beta(\varphi) \\ -\sin\beta(\varphi) & \cos\beta(\varphi) \end{pmatrix}, \tag{3.10}$$

where the closing angle β is the amount of "deformation" that is needed to twist the trajectories of DS($\mathcal{K}$) to closed orbits. The magnitude of this deformation is quantified by the norm of the closing angle β and depends on the shape of the cycle family. On an invariant manifold the drift points exactly along the manifold and hence β vanishes. In the picture of the crosswind, on invariant manifolds no winds are blowing, since they already are closed orbits; see the inset of Fig. 3.3. Note, that $\mathcal{R}$ only changes the direction of the flow not its magnitude, hence

$$|\mathcal{L}| = |\mathcal{R}\mathcal{K}| = |\mathcal{K}|. \tag{3.11}$$

We may call this 'energy preserving'.

The closing angle β can be explicitly determined for a cycle family $\mathcal{C}$ by comparing the direction of the flow between $\mathcal{L}$ and $\mathcal{K}$, that is

$$\beta(\varphi) = \arcsin\left(\frac{\mathcal{L}(\varphi) \times \mathcal{K}(\varphi)}{|\mathcal{L}(\varphi)||\mathcal{K}(\varphi)|}\right) = \arcsin\left(\frac{\mathcal{L}(\varphi) \times \mathcal{K}(\varphi)}{|\mathcal{K}(\varphi)|^2}\right), \tag{3.12}$$

where $\times$ is the cross product of two vectors. We note here why the sine is used: If we would use the cosine, which is symmetric around the origin, we would not have a sign change when crossing the stable invariant manifold. But the crosswind should change its sign when crossing a stable invariant manifold to stop trajectories from ending in the manifold.

[4]It does not matter whether rotations clock- or counterclockwise are used, it would only change the sign of the closing angle and therefore is only conventional.

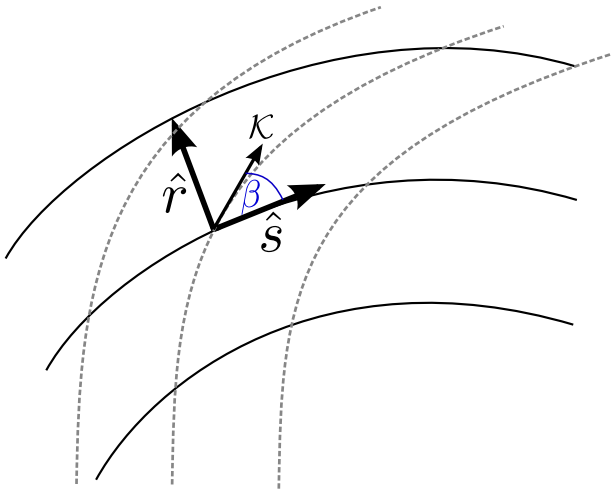

Figure 3.4: Shown are some cycles of the DS($\mathcal{L}$) (solid black lines) and the drift field DS($\mathcal{K}$) (dashed gray lines). The local curvilinear coordinates (r, s) are locally tangential to the cycles. The closing angle β (in blue) between the drift vector $\mathcal{K}$ and cycle tangent $\hat{s}$ is shown as well.

3.1.2.1 Coordinate transformation

This subsection is more a technical interlude about different representations of a position in either the original phase space and the continuous cycle space. For simplicity we restrict ourselves to the two-dimensional case. Let the position in the phase space be given by $\varphi = (x, y)$ in the global (x, y) phase space coordinate system. For a given cycle family, i.e., a set of closed curves parameterized by their projections p onto the $\hat{p}$-axis we can use mainly two different representation of φ: a parametric representation as well as local curvilinear coordinates.

The parametric representation uses the cycle family parameter p and the "completion time" τ, which is the normalized period time of the cycle associated with p. Hence any position φ can be represented with the tuple $(\tau; p)$ or more explicitly

$$\varphi = \gamma(\tau; p), \tag{3.13}$$

where $\gamma(p)$ is the trajectory of the cycle associated with paramter p. Equivalently, we sometimes use the position s on a cycle, which can also be normalized to the cycle length. The relation between the two representations reads, $\mathrm{d}s = |\mathcal{L}(s)|\mathrm{d}\tau$.

The local coordinate system is defined by two vectors: the local tangent and normal unit vectors, $\hat{s}$ and $\hat{r}$, respectively. The tangential points along the flow, parallel to $\mathcal{L}$, on the cycle and hence locally spans $\hat{s}$. A corresponding orthogonal coordinate is denoted with $\hat{r}$ and is defined to point in the direction of increasing p. The local frame is therefore called (r, s)-system.

3.2 Towards a NESS potential

In this section we want to develop explicit formulas for a candidate ansatz of a NESS potential as presented by [31]. The full procedure can be summarized as follows. A more detailed description of the each step follows afterwards.

(I) Determine drift and diffusion fields, $\mathcal{K}(\varphi)$ and $\mathcal{D}(\varphi)$, from the microscopic dynamics.

(II) Find the invariant manifolds of the corresponding dynamical system DS($\mathcal{K}$).

(III) Choose an axis intersecting invariant manifolds analogously to the Poincaré section. We may call this axis $\hat{p}$ and introduce a parameterization p.

(IV) Perform a cycle transformation of the phase space, that is:

  a) find a suitable family of cycles containing the invariant manifolds;

  b) determine the crosswind operator $\mathcal{R}$ along each cycle.

(V) Calculate the transition rates between neighboring cycles from $\mathcal{R}$ and $\mathcal{D}$.

(VI) Integrate the logarithm of the transition rates along p to obtain a potential difference between the invariant manifolds.

Theoretically, the drift and diffusion field, $\mathcal{K}$ and $\mathcal{D}$, for step (I) could be found from analyzing experimental data, see for example the approach presented by Battle *et al.* [6]. But here for the first test of validity of this ansatz, we use known dynamical systems. This avoids the additional error source of evaluating experimental data. The criteria of selection of the dynamical systems are that they be two dimensional and posses a stable limit cycle with a single unstable node enclosed by the stable manifold and no other attractors or repellers. For the used systems and their details please refer to Sec. 3.3. Consequently, from the known dynamics the trajectories of the drift field can be obtained by (numerical) integration of the corresponding dynamical system DS($\mathcal{K}$). How we performed this numerical calculations will be discussed in Sec. 4.1.

The invariant manifolds in step (II) can be determined from long time observation and may reach stationary dynamics of the system either from long time experiments or, in our case, from long time integrations. Please see Sec. 4.1.2 for how the invariant manifolds are numerically determined.

To choose the $\hat{p}$-axis we need to make sure that it fulfills the required properties as described in Sec. 3.1.1. We only use systems with a topology that allows us to define a straight line from the enclosed fixed point to the surrounding limit cycle. For simplicity we choose $\hat{p}$ parallel to the x-axis of the phase space and place the origin, $p = 0$, on the fixed point; we chose units such that the limit cycle has coordinate $p = 1$.

Step (IV) will be discussed in Sec. 4.2. The last points (V) and (VI) need a bit more elaboration, which is presented in the following section.

3.2.1 Computing the potential

Now we want to give explicit formulas of the candidate ansatz for a NESS potential. This equation set is adapted from [31]. To idea is to find a way to quantify the transitions between neighboring cycles from the diffusivity $\mathcal{D}$ and crosswind operator $\mathcal{R}$ without solving the original Master equation.

To compute the transition rate $v_{\beta\alpha}$ between two neighboring cycles from cycle α directed to β, the densities of systems ρ_α on these cycles is considered. By definition, the cycle weights or currents c_α need to be constant along a cycle. Thus, we can write [31]

$$\rho_\alpha(s)|\mathcal{L}(s)|\delta r(s) = c_\alpha = \text{const.}, \tag{3.14}$$

where δr is the locally orthogonal distance between the cycle, and s the arc length along a cycle; for the definition of the curvilinear coordinates see Sec. 3.1.2.1. Equation (3.14) is the continuity equation for the flux along a cycle α. For the continuous cycle space we replace the discrete enumeration of cycles with a continuous parameter, that is chosen to be the p parameter, as discussed in Sec. 3.1.1. Rewriting Eq. (3.14) into a continuum version by defining $c_\alpha \equiv \delta p\, c(p)$, yields

$$c(p) = \rho(p,s)|\mathcal{L}(p,s)|\frac{\mathrm{d}r}{\mathrm{d}p}. \tag{3.15}$$

Because we aim to provide a first test of our ansatz for a NESS potential, we now make a simplification: we assume the diffusion matrix $\underline{\underline{D}}$ to be the identity matrix, i.e. $\underline{\underline{D}} = \mathcal{D}\underline{\underline{\mathbb{I}}}$, with scalar diffusion constant $\mathcal{D}$. This can be seen as isotropic diffusion, which may be considered artificial but has the benefit that the diffusion matrix remains the identity matrix under transformation into the local coordinates (r,s) with an orthogonal matrix. We note that other forms of $\underline{\underline{D}}$ are possible.

Hence transitions between the cycles due to diffusion occur in $\hat{r}$-direction. With the above simplification this can be written as $J^D \equiv \underline{J}^D \cdot \hat{r}$. Furthermore in (r,s)-coordinates the gradient of ρ reads,

$$\nabla_{(r,s)}\rho \cdot \hat{r} = \frac{\partial \rho}{\partial r} = \frac{\partial \rho}{\partial p}\frac{\partial p}{\partial r} \equiv \frac{\partial \rho}{\partial p}|\nabla_{(r,s)}p|, \tag{3.16}$$

where we treat p as a scalar field, whose contour lines coincide with the cycles of the chosen cycle family. For readability, we drop the indices of the gradient and note that all gradient in this section are in local (r,s)-coordinates. Hence the gradient of p points in direction of $\hat{r}$.

The diffusion in $\hat{r}$-direction is according to Eq. (3.6) at position s,

$$J^D(s) = -\mathcal{D}(s)\left[\nabla\rho(s)\cdot\hat{r}\right], \tag{3.17}$$

and integrated over a cycle, $\gamma(s;p)$,

$$J^D = -\oint \mathcal{D}(s)\frac{\partial\rho(s)}{\partial r}\mathrm{d}s = -\oint \mathcal{D}(s)|\nabla p(s)|\frac{\partial\rho(s)}{\partial p}\mathrm{d}s, \tag{3.18}$$

where Eq. (3.16) is used. The integrals in Eq. (3.18) are line integrals over the trajectory $\gamma(s;p)$.

From Eq. (3.15) one gets, when also treating p as scalar field,

$$\rho(p,s) = \frac{c(p)|\nabla p|}{|\mathcal{L}(p,s)|}. \tag{3.19}$$

Hence the derivative of ρ with respect to p reads,

$$\frac{\partial \rho}{\partial p} = \frac{\nabla p}{|\mathcal{L}|}\frac{\partial c(p)}{\partial p} + c(p)\frac{\partial}{\partial p}\left(\frac{|\nabla p|}{|\mathcal{L}|}\right). \tag{3.20}$$

Inserting this into Eq. (3.18) yields,

$$J^D(p) = -\oint \mathcal{D}(s)|\nabla p|\left[c'\frac{|\nabla p|}{|\mathcal{L}|} + c\left(\frac{|\nabla p|}{|\mathcal{L}|}\right)'\right]\mathrm{d}s, \tag{3.21}$$

where the primes denote differentiation with respect to p.

The flux normal to a cycle of $\mathrm{DS}(\mathcal{L})$ is given by the sine of the angle of the crosswind β. It reads

$$J^K(p) = \oint \sin\beta(p,s)\rho(s)|\mathcal{L}(s)|\mathrm{d}s = \oint \sin\beta(p,s)c(p)|\nabla p|\mathrm{d}s, \tag{3.22}$$

where Eq. (3.19) is used again and integration is over the cycle, $\gamma(s;p)$, at p.

By using detailed balance condition between the cycles, which reads $J^D + J^K = 0$, we obtain by using Eq. (3.21) and (3.21),

$$c'\oint \mathcal{D}|\nabla p|^2\frac{\mathrm{d}s}{|\mathcal{L}|} = c\oint\left[\sin\beta - \mathcal{D}\left(\frac{|\nabla p|}{|\mathcal{L}|}\right)'\right]|\nabla p|\mathrm{d}s. \tag{3.23}$$

Equation (3.23) is a differential equation for c, whose solution reads

$$c(p) = c_0\exp\left(\frac{\oint\left[\sin\beta - \mathcal{D}\left(\frac{|\nabla p|}{|\mathcal{L}|}\right)'\right]|\nabla p|\mathrm{d}s}{\oint \mathcal{D}|\nabla p|^2\frac{\mathrm{d}s}{|\mathcal{L}|}}\right). \tag{3.24}$$

Compared to (3.3) the potential Φ is finally given by

$$\Phi(p) = -\ln\left(\frac{c(p)}{c_0}\right). \tag{3.25}$$

3.3 Dynamical systems

In this section we want to introduce the dynamical systems used for the numerical testing of our cycle transformation approach. For this first test, we restrict ourselves

to two-dimensional systems. This enables us to use the Poincaré-Bendixon theorem (see Sec. 2), which states that in two dimensions fixed points and limit cycles are the only possible attractors. Because we want to connect two invariant manifolds we choose some systems with simple topology, i.e., dynamical system with a single unstable equilibrium enclosed in a attracting limit cycle. Namely, we used the van-der-Pol oscillator and the Brusselator. Furthermore, we restrict ourselves to autonomous dynamical systems. The required properties of those systems will be presented in the following.

3.3.1 van-der-Pol Oscillator

The van-der-Pol equation was first derived to describe nonlinear electrical circuits used in the first radios. A realization is a so-called van-der-Pol oscillator. The van-der-Pol equation can also be used to analyze wind-induced oscillations in buildings and general aeroelastic flutter problems [25]. The analysis of the van-der-Pol equation played an essential role in the development of the dynamical systems theory. The van-der-Pol equation reads

$$\ddot{x} + \mu(x^2 - 1)\dot{x} + x = 0, \tag{3.26}$$

where the vanishing r.h.s. corresponds to the unforced van-der-Pol oscillator and μ is a damping constant. The van-der-Pol oscillator is like a harmonic oscillator with non-linear damping term. Settings $\mu = 0$ gives us a harmonic oscillator. The non-linear damping in Eq. (3.26) implies, that for $|x| > 1$ we have normal damping leading to decaying amplitude and for $|x| < 1$, negative damping, that is, self-driving. The first one leads to energy dissipation and the last one to driving. Balancing the loss and gain of energy of the van-der-Pol oscillator give rise to a stable limit cycle. It can be shown that such limit cycle exists for all $\mu > 0$ [22, 25].

The phase plane in the left panel of Fig. 2.1 shows the phase space representation of Eq. (3.26) which is

$$\begin{pmatrix} \dot{q}_1 \\ \dot{q}_2 \end{pmatrix} \equiv \begin{pmatrix} \dot{x} \\ \ddot{x} \end{pmatrix} = \begin{pmatrix} q_2 \\ \mu(1 - q_1^2)q_2 - q_1 \end{pmatrix}. \tag{3.27}$$

Eq. (3.27) defines a two dimensional dynamical system for the van-der-Pol oscillator, $\dot{q} = F(q)$, with $q = (q_1, q_2)^{\mathrm{T}}$. A stability analysis of Eq. (3.27) reveals a single fixed point at the origin. In the harmonic case the fixed point becomes a center, which we expect for a harmonic oscillator. For $\mu < 0$ the fixed points becomes stable, for $0 < \mu < 2$ an instable focus and for $0 \leq \mu < +\infty$ an instable node. Since there are no other fixed points and we know that there is a single stable limit cycle γ_{LC} for $\mu > 0$, we know that $\gamma_{\mathrm{LC}} = \omega(\mathbb{R}^2 \setminus 0)$. As remider, ω is the limit set that is reach forwards in time. In other words we will for positive μ end in the limit cycle if start anywhere but not in the origin [24].

3.3.2 Brusselator

The so-called "Brusselator" is a model for autocatalytic chemical reactions studied by Nicolis and Prigogine [10], who are known as the Brussels school. An autocatalytic reaction is one that has the same chemical species on the product and as well on reactant side, e.g. [32]

$$\mathrm{A} + \mathrm{X} \rightarrow 2\mathrm{X}.$$

The reaction described by the Brusselator reads

$$\begin{aligned} \mathrm{A} &\rightarrow \mathrm{X} \\ 2\mathrm{X} + \mathrm{Y} &\rightarrow 3\mathrm{X} \\ \mathrm{B} + \mathrm{X} &\rightarrow \mathrm{Y} + \mathrm{D} \\ \mathrm{X} &\rightarrow \mathrm{E}. \end{aligned}$$

If we constantly supply A and B and remove D and E these reactions can be mainted far from equilibrium by eliminating some backreactions. Setting the rate of the backreactions to zero and, for simplicity, the rate constants to unity, we arrive at the rate equations [32, 33]

$$\dot{x} = \alpha + x^2 y - (\beta + 1)x \tag{3.28}$$

$$\dot{y} = \beta x - x^2 y. \tag{3.29}$$

x and y are the concentrations of the reactants and α and β describe the supply of the according chemicals. We interpret this a two-dimensional dynamical system. It has a unique fixed point at $(\alpha, \beta/\alpha)$, which is stable for $0 < \beta \leq \alpha^2 + 1$ and then the global attractor. At $\beta = \alpha^2 + 1$ the system possesses a Hopf bifurcation, which gives rise to a stable limit cycle. The limit cycle is the global attractor (without the fixed point) for $\beta > \alpha^2 + 1$.

We generally use the parameter set $(\alpha, \beta) = (1, 3)$. Thus, the fixed point resides at $\varphi_{\mathrm{FP}} = (1, 3)$. The phase space with the fixed point and limit cycle are shown in Fig. 2.1.

Chapter 4

Numerical concepts and implementation

Now we want to focus onto numerical aspects and the implementation of the candidate ansatz for a NESS potential that is presented here.

4.1 Solving Dynamical Systems

For any further analysis and application of the cycle transformation we need to have a solution or trajectories of the dynamical system. We especially need their long-time limit, which are the invariant manifolds. Since analytic solution for non-linear dynamical systems rarely exist, we need to find the solution by numerical integration. With the decoupling between diffusivity caused by noise and drift described by dynamical systems, see Sec. 3.1.1, we are able to use deterministic integrators.

4.1.1 Integration with the Dormand-Prince method

The integration method we mainly use for solving dynamical systems is the so-called *Dormand-Prince method* (DOPRI) [34]. This method belongs to the family of explicit Runge-Kutta methods with order (4)5. It supports stepsize control and dense output. It is best suited for low tolerances in the range of 10^{-4} to 10^{-7} [35]. If we need even lower tolerances the DOPRI8 subroutine is used instead, which is a DOPRI of order 8 with good results for tolerances between 10^{-7} to 10^{-12} [35]. The DOPRI 4(5) method uses six evaluations per step because the last step of the previous equals to first of the following evaluation. The local error is defined as the difference between the fourth- and fifth-order approximations and used for stepsize control. Based on this local error, the stepsize is adjusted to gain results within a certain accuracy when using dense output. In regions of high curvature a shorter stepsize is used and vice versa.

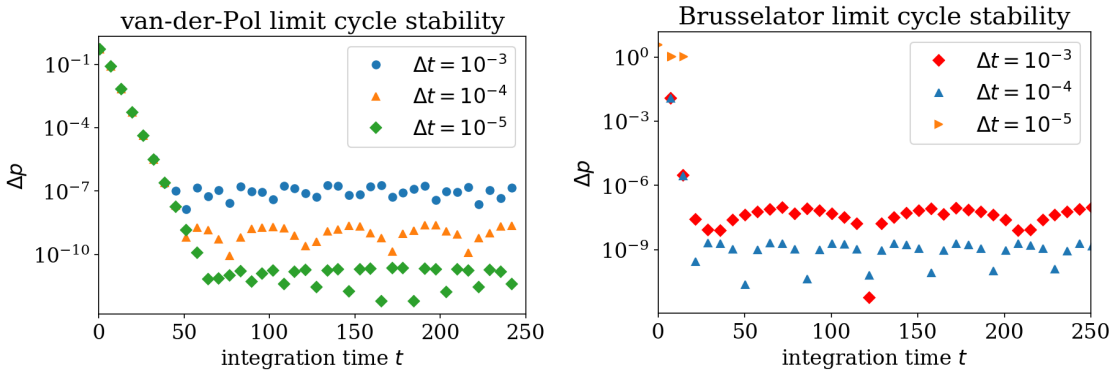

Figure 4.1: Distance Δp between to successive $\hat{p}$-intersections of the integrated limit cycle for the van-der-Pol oscillator (*left*) and Brusselator (*right*). We see that they converge exponentially in the so-called transition time and then reach a certain level dependent on the time step Δt. The integration of the Brusselator for $\Delta t = 10^{-5}$ becomes unstable.

One major advantage of the DOPRI method is the ability to make a fourth order continuous expansion even without any additional function evaluation [35], the so-called dense output. That are points between one time-step dt, whose values can be obtained without any additional computational costs. The can be used to increase precision of the calculated solution. A description of the used implementation of the DOPRI method can be found in the appendix of [35].

4.1.2 Invariant Manifolds

In this thesis we solely deal with dynamical systems (see Sec. 3.3), whose invariant manifolds are a stable limit cycle and enclosed unstable fixed point. The existence of the enclosed fixed point is ensured by Theorem 2 but we need to find it with analytical tools. The stable limit cycle is an ω-limit set, see Sec. 2.2.3. Hence to find the ω-sets we need to do long-time integrations. Unfortunately, for numerical integration we need some finite integration time and need to verify whether these are chosen sufficiently long. Therefore we check the convergence of the difference of two $\hat{p}$-axis intersection of successive iterations. We expect them to converge to a constant. If this constant if small enough, we accept the integration time of ω-set as adequately.

Whether we will end up in the limit cycle or stay in a fixed point is a question of initial condition. But since the limit cycles are the only attractors, any initial condition that is not of zero measure, e.g. a fixed point, will end in the limit cycle.

The solutions found are stored for further analysis, calculation of the cycle transformation and for the test of the path independence. See Fig. 2.1 for examples of the obtained limit cycles and fixed point in phase space.

4.2 Cycle Families

Now with the solutions of the dynamical system at hand, we can perform a cycle transformation as introduced in Sec. 3.1. For this we need first to choose a connecting axis of the invariant manifolds, the $\hat{p}$-axis. For simplicity we use an axis parallel to the x-axis of the phase space on the y-value of the fixed point.

For any further computations, we need to have the trajectory of only one period, so that any point is only included once. For the fixed point this is easy but the long-time integrations of the limit cycles need to be reduced to one period. This is achived by searching the last two intersections of the limit cycles data with the $\hat{p}$-paxis and cut-off the rest. Since we normally 'overshoot' the $\hat{p}$-axis, due to finite time steps, we correct this with linear interpolation onto it.

In what follows we will elaborate ways to define and numerically find different paths through the cycle space, i.e., a cycle family. As a reminder of Sec. 3.1.1, the requirements for a cycle family are that they (i) fill the full phase space[1] (ii) do not intersect, and (iii) are smooth. The first two points are required for the p projection to be unique. Smoothness is required here because we need tangential vector, e.g. to determine the closing angle β. If the cycles where not smooth everywhere, there would exist a position, where no derivative and hence tangent vector exist.

We use different techniques to find such families. Those can be categorized into two categories by their underlying theory, which we call the *cycle-constant crosswind*- and *homotopy*-families.

4.2.1 Cycle-Constant Crosswind operator

In this section we show that one can find a single closing angle β that is constant along a cycle or equivalently one β for each parameter value p. Hence we show that $\beta = \beta(p)$ and $\beta(p, s) = \text{const.}$ along s.

That such an angle β exists is based on the idea that trajectories of DS($\mathcal{K}$) are unique. Especially they cannot cross each other. Hence, applying the crosswind operator with a constant β globally defines, analogously to Sec. 3.1.2, a new dynamical system DS($\mathcal{L}$). If we do an integration of DS($\mathcal{L}$), which starts at p_0 on the $\hat{p}$-axis, the first intersection with the $\hat{p}$-axis is unique as well, if it exists. Thus, we can define a function for any given initial p-value, p_0, that gives us the first intersection, p_1, in DS($\mathcal{L}$). Let's call this function P. It depends on the starting point p_0 (this dependence is indicated as a subscript) and the angle β used to define DS($\mathcal{L}$). We fix one p_0 and write

$$P_{p_0}(\beta) = p_1. \tag{4.1}$$

Due to uniqueness of the solutions of DS($\mathcal{L}$), P can be inverted, if p_1 exist. This gives us the angle needed to be applied to reach p_1 when starting at p_0

$$\beta = P_{p_0}^{-1}(p_1). \tag{4.2}$$

[1] Or at least the area between the invariant manifolds and sufficiently large domain to see the extrema of the potential.

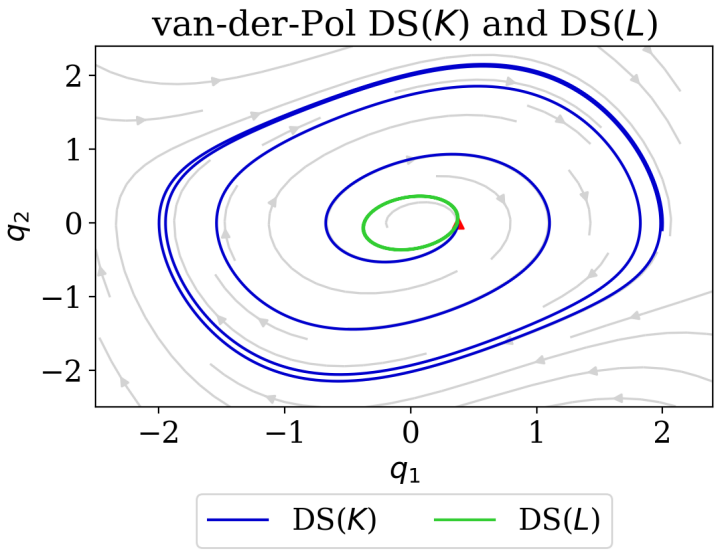

Figure 4.2: Limit cycle of the original van-der-Pol oscillator dynamical system, DS($\mathcal{K}$), and one cycle of DS($\mathcal{L}$). Both trajectories start at the same position in phase space depicted by the red triangle. The streamlines of DS($\mathcal{K}$) are shown in light-gray. We see that without the crosswind operator applied, which is DS($\mathcal{K}$), the trajectories would spiral towards the limit cycle of DS($\mathcal{K}$).

To close a trajectory we now evaluate P^{-1} numerically and find the closing angle $\bar{\beta}$

$$P_{p_0}^{-1}(p_0) = \bar{\beta}, \tag{4.3}$$

i.e., the starting position and the first intersection on the $\hat{p}$-axis are equal. The validity of the results can be verified by checking if P^{-1} vanishes on stable invariant manifolds.

The numerical evaluation is realized as an inversion problem. For a given p_0 the first intersection is determined for several β values and the root of the equation

$$\Delta p_{p_0}(\bar{\beta}) \equiv p_0 - p_1 = p_0 - P_{p_0}(\bar{\beta}) = 0, \tag{4.4}$$

is searched. The root at $\bar{\beta}$ corresponds to a closed orbit. Thus, we can determine a map that gives the required crosswind angle β for a given intersection value p, which we call the $\beta - p$-map.

From a computational point of view, this is done by using binary search, which shows fast convergence towards the root. The basic algorithm can roughly be described as:

(i) Evaluate P_{p_0} for N different values of $\beta \in [-\pi, \pi]$,

(ii) determine the β's closest to the root, β_- and β_+,

(iii) halve the interval $\beta_m = \frac{1}{2}(\beta_- + \beta_+)$ and calculate $p_1(\beta_m)$,

(iv) update the boundaries with if $p_0 - P_{p_0}(\beta_m) < 0$, set $\beta_+ = \beta_m$, else $\beta_- = \beta_m$.

(v) Repeat steps (iii)-(iv) until given precision $\Delta\beta_{\text{tol}} \equiv \beta_+ - \beta_-$ is reached.

Note that we can determine the closing angles β for our sample space on p by parallel calculations, since they do not depend on each other.

Once β is calculated, we check the correctness by verifying that the limit cycle is stable on the corresponding p value. Therefore we determine the distance off the intersections with the $\hat{p}$-axis by integrating for several hundreds periods, analogously to Sec. 4.1.2.

4.2.2 Homotopy

Up to this point, we have dealt with crosswinds that are constant along a cycle and thus depend only on p. We now want to introduce a simple method to find a cycle family, whose crosswind depends on the position on the cycle. For this purpose we use homotopy.

If two continuous curves, $\gamma_0, \gamma_1 : [a, b] \to X$, on the same space X can be "continuously deformed" into each other, these curves are called to be homotopic. The continuous mapping between those is said a homotopy H. It is defined as [27]

$$H : [a, b] \times [0, 1] \to X, \tag{4.5}$$

with the time domain $t \in [a, b]$ of the two curves and $p \in [0, 1]$ the transformation parameter; the homotopy needs to satisfy

$$\begin{aligned} H(t, 0) &= \gamma_0(t)\, \forall t, \\ H(t, 1) &= \gamma_1(t)\, \forall t, \\ H(a, p) &= H(b, p)\, \forall p. \end{aligned}$$

Because we solely deal with closed orbits with a finite period time, the trajectories' time domain can always be normalized with the period time, such that $t \in [0; 1]$. There are infinite many mappings that fulfill the above conditions. We will differentiate between two general concepts: the so-called *linear* and *chained homotopy*, which will be introduced below.

We will use homotopy to transform the (stable) limit cycle into the enclosed (unstable) fixed point[2]. Evaluating H at a discrete set of p's, gives us numerically a discrete cycle family.

4.2.2.1 Linear Homotopy

We call a homotopy between two curves, γ_0 and γ_1, *linear* or *straight-line homotopy* if it is given by

$$H(t, p) = p\gamma_0(t) + (p - 1)\gamma_1(t). \tag{4.6}$$

[2] A fixed point is here a curve, which is constant in time.

As the name suggests, the two curves are transformed into each other on a straight lines between the points of each curve corresponding to equal times.

Equation (4.6) can be numerically implemented straightforwardly once the position of the fixed point and trajectory of the limit cycle are determined. However, by setting γ_1 to be the fixed point and γ_0 the limit cycle, the homotopy would only transform the fixed point into the limit cycle. In order to see an extremum in the resulting potential at the stable limit cycle for this cycle family we need to include values for $p \geq 1$. To resolve this issue, the homotopic transformation is carried out with the following algorithm:

(i) translate the fixed point γ_1 into the origin $\gamma_1' = 0$,[3]

(ii) apply the translated homotopy H' on the limit cycle γ_0

$$H'(t, p) = p\gamma_0(t), \tag{4.7}$$

(iii) translate back into original space.

This algorithm only works if one curve is constant, i.e., a fixed point. We can think of this transformation as uniformly "shrinking" a limit cycle into an enclosed fixed point.

When the cycle family is determined, we need to evaluate the closing angle β, i.e., the angle between the drift vector of DS($\mathcal{K}$) and the tangential vector of the cycles of the family, in order to determine the potential. β can be calculated with Eq. (3.12). Thus, we need the cycle tangential vectors $\mathcal{L}(\varphi)$ and $\mathcal{K}(\varphi)$. The latter is directly obtained from the dynamical system definition and the former by using a small trick: since we are applying a *straight-line* homotopy, i.e., a multiplication of the distance vector between the fixed point and point on the limit cycle, the associated tangent does not change its direction. Consequently, we can use the corresponding drift vector of the limit cycle as $\mathcal{L}$. The magnitude of the drift instead changes, but with $|\mathcal{L}(\varphi)| = |\mathcal{K}(\varphi)|$ from Eq. (3.11) we can find the correct magnitude at φ.

[3]The primes denote the translated relations.

Chapter 5

Testing of the NESS potential

In this chapter we describe the results we obtain when we apply the procedure for a candidate NESS potential, as introduced in Sec. 3.2. We start with the van-der-Pol oscillator in Sec. 5.1 and then also apply the procedure to the so-called Brusselator in Sec. 5.2.

5.1 Van-der-Pol Oscillator

We start by evaluating the van-der-Pol oscillator with the nonlinearity parameter μ fixed, since we are not interested in bifurcation behavior here. As discussed in Sec. 3.3.1, for $\mu \in]0, 2[$ there exists a single unstable fixed point in the origin and an otherwise globally attractive limit cycle. The limit cycle represents the nonequilibrium steady state of the system. The phase space with fixed point and limit cycle is shown in Fig. 2.1. We have thus two invariant manifolds: the unstable fixed point at the origin and the limit cycle around as the stable invariant manifold.

For our ansatz of a NESS potential, presented in Sec. 3.2.1, we assume a constant and isotropic diffusion tensor $\underline{\underline{D}}$, i.e., $\underline{\underline{D}} = \mathcal{D}\underline{\underline{\mathbb{I}}}$ with a scalar diffusion constant $\mathcal{D}$ and identity matrix $\underline{\underline{\mathbb{I}}}$. Choosing values for the diffusion constant $\mathcal{D}$ is challenging since in equilibrium it is given by the Einstein-Smoluchowski relation, $\mathcal{D} \propto k_B T$, with Boltzmann factor k_B and temperature T. But there is no well-defined temperature T for nonequilibrium steady states so that leaves the open question of how to choose $\mathcal{D}$. In practice, we choose $\mathcal{D}$ such that the dynamics of DS($\mathcal{K}$) are not washed up by the noise, which provides an upper bond, to $\mathcal{D}$ and also such that the non-vanishing transitions among the cycles take place, which provide a lower bond. The used values are indicated in Fig. 5.3. Note that all quantities used are in dimensionless form. With that we have completed step (I) of the procedure.

Continuing with step (II) (finding of the invariant manifolds), the fixed point is found by analytical treatment, see Sec. 2.2.2. We discussed in Sec. 4.1 how the differential equations of the van-der-Pol oscillator have been numerically integrated.

The DOPRI integration method employed here leaves us some choices to make, i.e., integration time T and time step Δt. Hence we need to find parameters that balance the precision, i.e. time step, integration time limit T and its needed computation time. In Fig. 4.1 we see the differences of intersections, Δp, with a $\hat{p}$-axis[1] of two successive periods of the limit cycle for different Δt. We see that Δp decays exponentially in the transition time and converges to a value depended on Δt. It fluctuates around a certain level, which we may call precision. For $\Delta t = 10^{-3}$ the fluctuations have a periodic shape. To be sure the solutions are not in the transition time, we use $T = 250$. Furthermore we use a time step $\Delta t = 10^{-3}$ since it is a good balance between precision, which is about 10^{-6} to 10^{-8}, and computation time. We define the maximal error, up to which we accept a cycle as closed, to the upper limit of the distances in Fig. 4.1 to $\Delta p_{\max} = 10^{-6}$.

The $\hat{p}$-axis for step (III), as already mentioned, is for comparability chosen to be parallel to the x-axis of the phase space. Its origin, $p = 0$, is the fixed point of the dynamical system DS($\mathcal{K}$). This definition for the $\hat{p}$-axis satisfies the required properties (unique intersection with every cycle at least in the considered region). See the bold black line in Fig. 5.1. Since the p-value are arbitrary we choose it to be the normalized distance between fixed point and limit cycle.

5.1.1 Cycles Families

We now want to perform the cycle transformation, which is step (IV), for the van-der-Pol oscillator. For that we use the introduced methods, which are the so-called *cycle-constant crosswind* and *linear homotopy*; see Sec. 4.2 for further details.

Firstly, we consider the cycle-constant crosswind family. In Fig. 5.1 some cycles of a cycle family created with that method are shown. The family is created with a constant increment Δp, i.e., the distance between neighboring cycles is constant. The limit cycle (red curve) and unstable fixed point (red triangle) are shown as well. We can observe that cycles can be formed when defining a new dynamical system $\mathcal{L} \equiv \mathcal{R}_\beta \mathcal{K}$, where $\beta = \text{const.} \, \forall \varphi$, $\mathcal{R}$ is the crosswind operator (see Sec. 3.1.2) and $\mathcal{K}$ the drift field of the van-der-Pol oscillator. $\mathcal{R}_\beta$ denotes here a crosswind operator that only depends on a constant angle β and not on position in phase space φ. Furthermore it can be observed that the shape of the cycles changes smoothly: around the fixed point ($p \ll 1$) the cycles appear of ellitical shape, while they convert into the shape of the limit cycle of DS($\mathcal{K}$) for $p \approx 1$, and for $p > 1$ (here depicted for $p_{\max} = 1.2$) the 'edges' become more emphasized. Also a decrease in distance between neighboring cycles for $p > 1$ can be seen on the long sides of the cycles.

By construction of the cycle-constant crosswind operator we have a unique closing angle β per cycle p. It depends solely on the cycle, given by p. The numerical results are shown in Fig. 5.2 for a family ranging from $p = 0$ to 1.2. As abort condition for the iteration step of the algorithm we allowed a tolerance of $\Delta\beta_{\text{tol}} = 10^{-8}$.

[1] Here it does not matter which exact axis is used since we only compare difference on the axis. But for consistency we also used a x-parallel one.

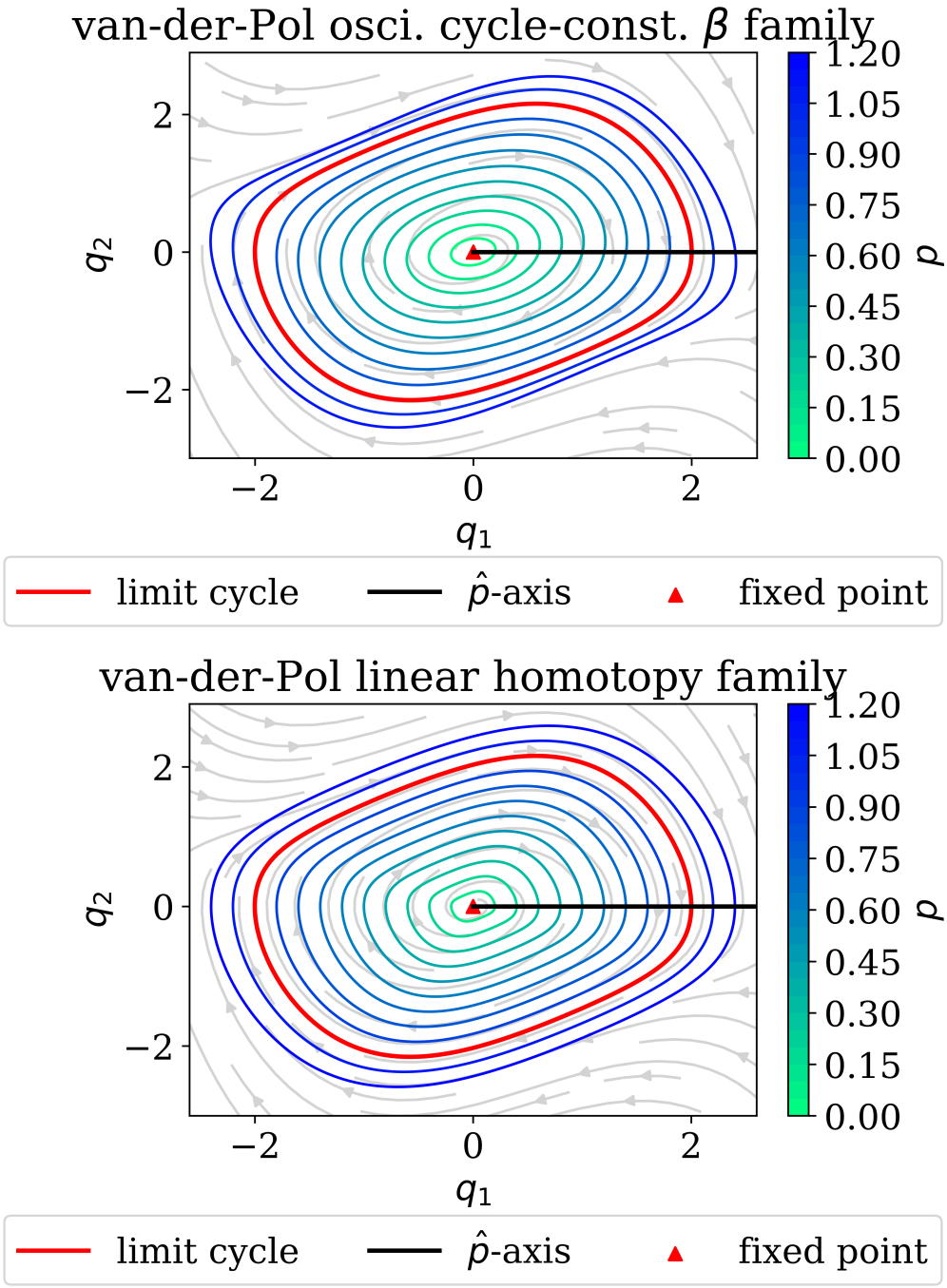

Figure 5.1: Cycle families of the van-der-Pol oscillator. Shown are some members (uniformly spaced on the $\hat{p}$-axis) generated with the *cycle-constant crosswind or* β (*top*) and *linear homotopy* (*bottom*) methods, see Sec. 4.2 for details. The coloring denotes the corresponding p-value of the cycle. The $\hat{p}$-axis (black line), limit cycle (red curve) and fixed point (red triangle) are shown as well. The light-gray lines show the streamlines of DS($\mathcal{K}$). The integration are carried out with $\Delta t = 5 \times 10^{-3}$ and an allowed tolerance of a closed cycle $\Delta p_{\max} = 10^{-4}$, see Sec. 4.1.2. For comparison of the families see Sec. 5.1.1.

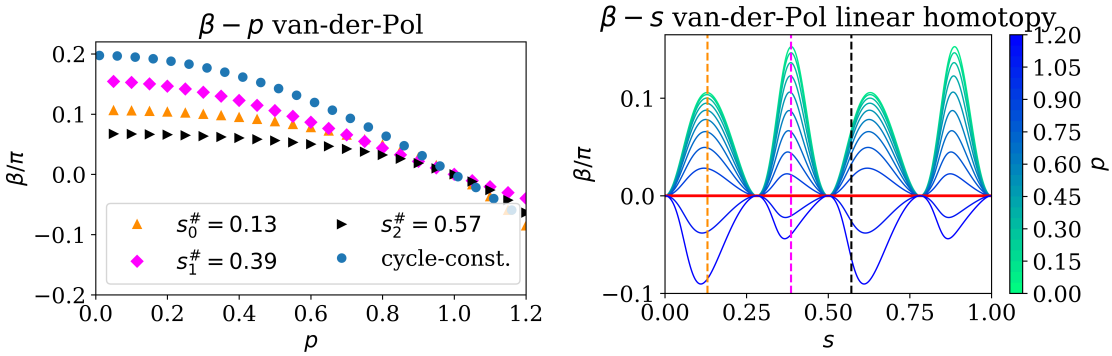

Figure 5.2: The closing angles β are shown as function of p (*left*) and as function of s for the linear homotopy family (*right*). We use the normalized arc length as position s. The color-coding in the $\beta - s$-plot indicates the p value of the corresponding cycle. The red line shows the limit cycle at $p = 1$. The vertical dashed lines correspond to the same colored graphs in the $\beta - p$ plot. The $\beta(p)$ map (blue dots) from the cycle-constant β family is shown as well. We see that $\beta(s; p = 1) = 0 \, \forall s$. The value $\beta(s; p = 0)$ is not defined for any s.

One sees that $\beta(p)$ decreases monotonically, with a maximum at $p = 0$, i.e., the fixed point, if $\beta(0)$ would be defined. Since $p = 0$ is a fixed point, by definition, the drift vanished (please note, that this hold for DS($\mathcal{K}$) as well as DS($\mathcal{L}$)). Hence $|\mathcal{K}| = |\mathcal{L}| = 0$ and consequently β is not well-defined there, see Eq. (3.12). Moreover, we note that for $p \to 0$, β does not approaches zero. The closing angle for the limit cycle vanished, $\beta(1) = 0$.

Secondly, we used the linear or straight-line homotopy as of Sec. 4.2.2. Some members of the obtained cycle family are shown in Fig. 5.1. Again, also the limit cycle of DS($\mathcal{K}$) (red curve) and fixed point (red triangle) are depicted. In direct comparison to the cycle-constant crosswind family one sees that the shape of the cycles constructed with homotopy is rather preserved.

In contrast to cycle-constant crosswind family the closing angle for the linear homotopy family depends upon position s on a cycle, i.e., $\beta = \beta(s; p)$. In other words for a given p a unique function $\beta(p)$ does not exist. Therefore we plot β over the normalized arc length s of a cycles for better comparison. See Fig. 5.2 for the results. The color indicates the corresponding p value. The red line shows β for $p = 1$, which is the limit cycle and is constantly zero along the limit cycle. We can observe that β does not changes sign for one p, but in a periodic manner going back to zero. The periodic behavior is due to the nearly symmetric drift field of the van-der-Pol oscillator. The zeros are caused by lines of the dynamical system, where the drift stays parallel, e.g. for the van-der-Pol the q_1-axis. The curves in Fig. 5.2 do not cross each other and keep their shape but are scaled for different cycles.

For a better comparison with the $\beta - p$-plot of the cycle-constant crosswind operator we plot $\beta(s^\#; p)$ for some fixed $s^\#$, which is then only function of p. The value of $s^\#$ is arbitrary, so we select a position where β is not identically zero. See the vertical lines in the $\beta - s$-plot in Fig. 5.2 for which values of $s^\#$ are used and the

corresponding $\beta(p)$ curves in the $\beta - p$-plot. We see that they have a comparable shape as the $\beta(p)$ from the cycle-constant crosswind. Furthermore they all intersect in $\beta(1) = 0$.

5.1.2 Candidate NESS potential

Finally, we address the last two steps (V) and (VI) and calculate a candidate NESS potential. We treat these two steps together since the equations in Sec. 3.2 are already cycle occupation densities $c(p)$. Our aims are to check whether a) the obtained potential for each family shows the expected properties and b) if the potential is path independent. The expected properties in a) are that the potential is maximal (repelling) in the unstable fixed point and minimal (attracting or stable) on the limit cycle. Moreover the path independence is fulfilled if for different families the potentials are equal in the extremal points, which are the invariant manifolds. To summarize, we now want to test if the potential has its maximum in $p = 0$, the fixed point, and minimum at $p = 1$, the limit cycle.

For this test we use the cycles families presented above. The results obtained from the equation (3.24) are shown in Fig. 5.3 for both families and different diffusion constants $\mathcal{D}$. Firstly, we see if the properties of a) are fulfilled. If we look at the shape of the potential $\Phi(p)$ separately, they have their maximum in the origin, decrease continuously to their minimum at $p = 1$, whose value depends upon $\mathcal{D}$. We note that the potential fulfills this for both families, i.e. for the cycle-constant crosswind and linear homotopy as well as for different values of $\mathcal{D}$.

To consider point b) we look at Fig. 5.3, where we see the differences of the potential $\Delta\Phi$ obtained from different paths, which we define as $\Delta\Phi(p) = \Phi_1(p) - \Phi_2(p)$, and for the same $\mathcal{D}$.[2] We see that they closely match (vanishing difference $\Delta\Phi$) for $p \approx 0$. For increasing p they diverge, which is caused by the different paths or families. The differences cross each other at $p \approx 0.7$. At the critical point, at $p = 1$ where the limit cycle is, the differences gain a local maximum, which is non-zero. We will discuss this results in Chapter 6.

5.2 Brusselator

In the above Sec. 5.1 we presented our results for the van-der-Pol oscillator of our candidate ansatz for a NESS potential. To test the robustness of our results with a different system, we now apply the same ansatz to the so-called Brusselator. For details on the system the reader is asked to refer to Sec. 3.3.2. We use the Brusselator with the parameters $\alpha = 1$ and $\beta = 3$ fixed. According to our discussion, the system then has an unstable fixed point at $(q_1, q_2) = (1, 3)$ in the phase space and a stable limit cycle around it.

[2] The choice which potential curve is Φ_1 or Φ_2 does not matter since we compare differences.

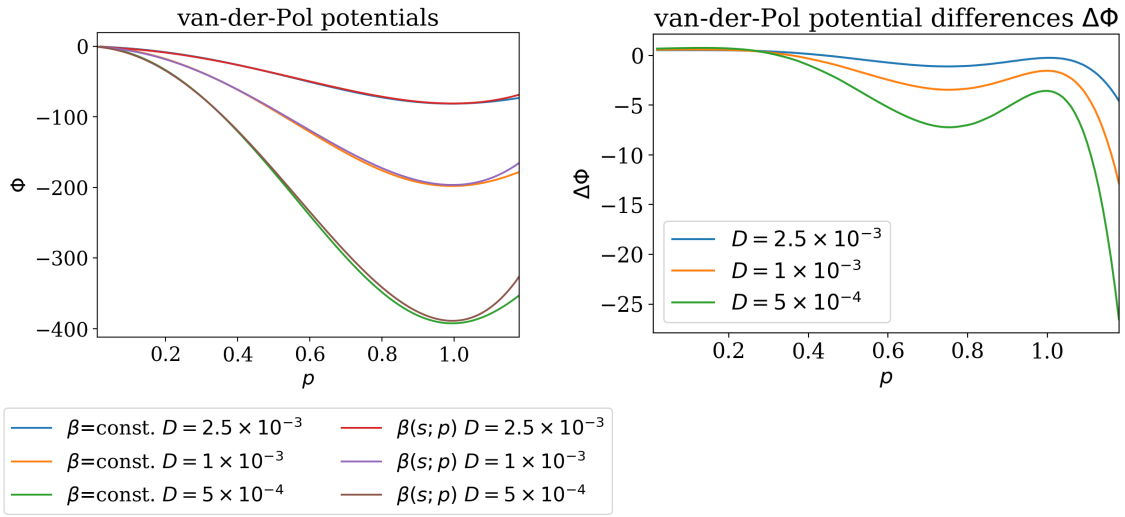

Figure 5.3: Numerical results for the above shown cycle families for a candidate NESS potential Φ for different values of the diffusion constant $\mathcal{D}$, see Sec. 3.2.1. $\beta =$ const. denotes the cycle-constant crosswind family and $\beta(s;p)$ the linear homotopy. To check expected properties and path independence the difference between the potential for a fixed $\mathcal{D}$ are shown as $\Delta\Phi \equiv \Phi_1 - \Phi_2$. The fixed point is a $p = 0$ and the limit cycle at $p = 1$.

In the following we apply the same procedure as for the van-der-Pol oscillator. In order to avoid duplication we ask the reader to look for more details on the approach in the above section.

The numerical integration to obtain the limit cycle was carried out with $T = 250$ and $\Delta t = 10^{-3}$. One can see in Fig. 4.1 that the stationary behavior then has been reached. The maximal error is $\Delta p_{\max} = 2 \times 10^{-5}$.

5.2.1 Cycles Families

Again, we use here the cycle-constant crosswind and linear homotopy cycle families as two different paths trough the cycle space. For consistency we define in the same manner the $\hat{p}$-axis to be parallel to the x-axis at the corresponding value of the fixed point.

At first, let us have a look at the cycle-constant crosswind family shown in Fig. 5.4. Depicted are some members of the cycles family. The color coding shows the p value of the cycle. The red line denotes the limit cycle of DS($\mathcal{K}$) and the red triangle the fixed point. Notable about the limit cycle is the 'sharp edge' with high curvature in its right most region. We see that the cycles smoothly change their shape likewise as for the constant crosswind family of the van-der-Pol oscillator. For low p values around the fixed point the cycles are like ellipses and evolve into the characteristic shape of the limit cycle of the Brusselator for increasing values of p. We also see that the distance between the cycles reduces on the 'short' sides of the

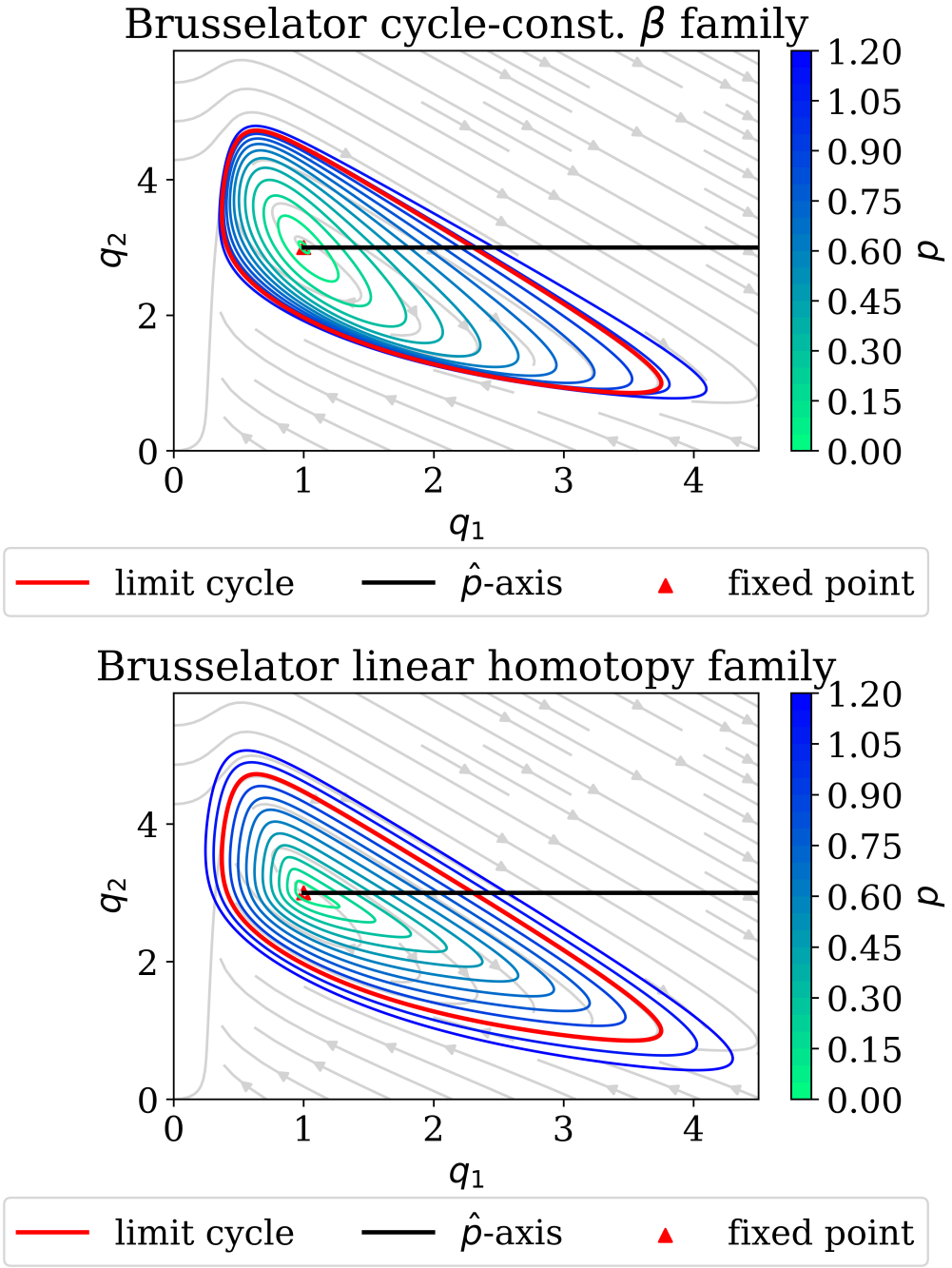

Figure 5.4: Cycle families of the Brusselator. Shown are some members (uniformly space on the $\hat{p}$-axis) generated with the *cycle-constant crosswind or* β (*top*) and *linear homotopy* (*bottom*) methods, see Sec. 4.2 for details.The coloring denotes the corresponding p-value of the cycle. The $\hat{p}$-axis (black line), limit cycle (red curve) and fixed point (red triangle) are shown as well. The light-gray lines show the streamlines of DS($\mathcal{K}$). The integration are carried out with $\Delta t = 5 \times 10^{-3}$ and an allowed tolerance of a closed cycle $\Delta p_{\max} = 10^{-4}$, see Sec. 4.1.2. For comparison of the families see Sec. 5.2.1.

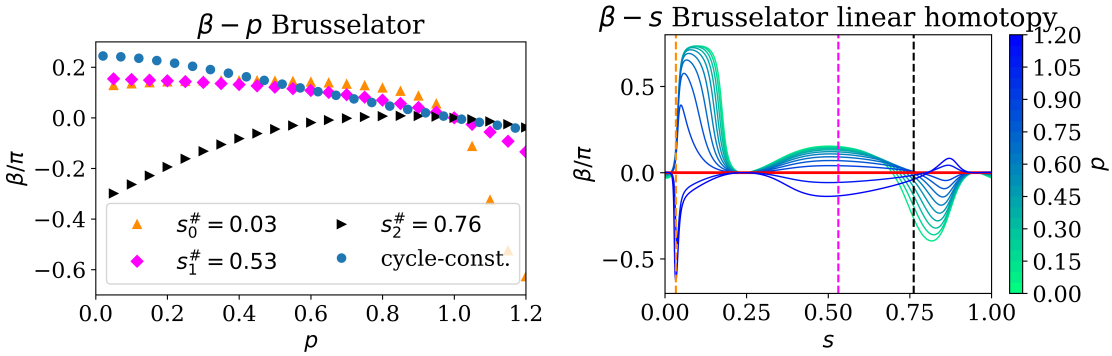

Figure 5.5: The closing angles β are shown as function of p (*left*) and as function of s for the linear homotopy family (*right*). We use the normalized arc length as position s. The color-coding in the $\beta - s$-plot indicates the p value of the corresponding cycle. The red line shows the limit cycle at $p = 1$. The vertical dashed lines correspond to the same colored graphs in the $\beta - p$ plot. The $\beta(p)$ map (blue dots) from the cycle-constant β family is shown as well. We see that $\beta(s; p = 1) = 0 \, \forall s$. The value $\beta(s; p = 0)$ is not defined for any s.

cycle for increasing values of p. This increase is caused by the streamlines of the original Brusselator, which are depicted in light-gray as well.

The cycle-constant closing angles $\beta(p)$ needed to close the trajectories are shown in Fig. 5.5. It has a comparable shape to the function obtained for the van-der-Pol oscillator. It starts for $p < 0$ with positive values, decreases monotonically and reaches zero at $p = 1$.

We continue with the cycle family generated with the linear homotopy method. This family is shown in Fig. 5.4 with limit cycle and fixed point in red. Again, by definition of the homotopy cycle generator, the distances for each s are constant over all cycles p (for uniformly spaced p-values). Also caused by the contraction is that the 'edges' for lower p values ($p \ll 1$) are more emphasized and become more curved.

The dependence on the archlengths of the crosswind angle $\beta(s; p)$ for this family is shown in Fig. 5.5. Most notably is that β along each cycle does have a sign change except for the constantly zero β for the limit cycle (red line). Also at some points the angles seek zero (without sign change). At low s-values, which correspond to the rightmost 'sharp edge,' the angles gain their greatest absolute value. As one sees the light-gray streamlines are nearly perpendicular to the cycle. Actually, as we see in Fig. 5.5, the closing angles are even greater than $\frac{\pi}{2}$. Analogously to the van-der-Pol the dependence of β upon p is shown for some fixed $s_i^\#$ in Fig. 5.5. We see that all curves go through $p = 1$ at $\beta(1) = 0$.

5.2.2 Candidate NESS potential

We now want to address the question whether our results are useful to identify a NESS potential. We proceed in the same manner as in Sec. 5.1.2. Therefore we

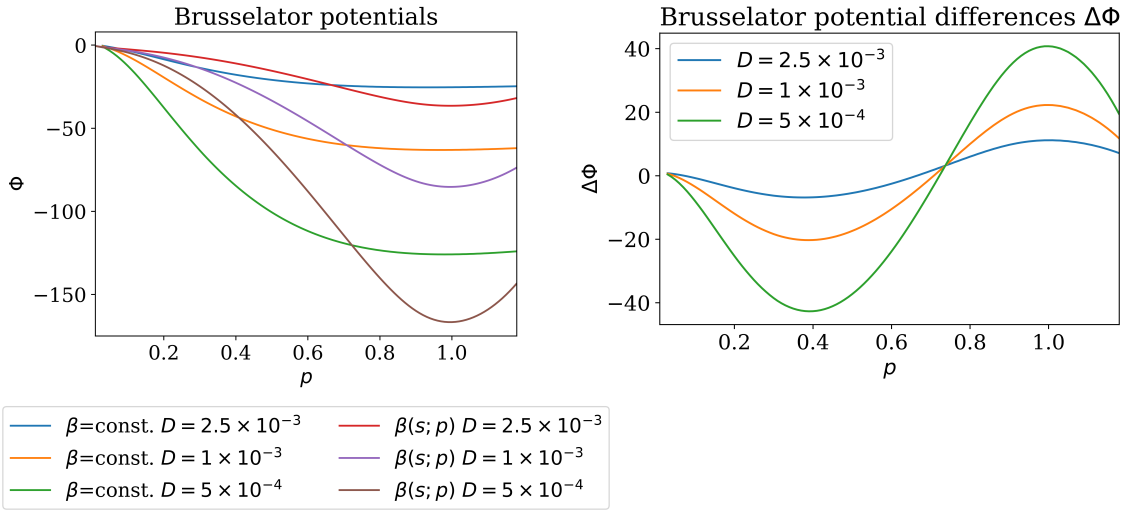

Figure 5.6: Numerical results for the above shown cycle families for a candidate NESS potential Φ for different values of the diffusion constant $\mathcal{D}$, see Sec. 3.2.1. $\beta =$ const. denotes the cycle-constant crosswind family and $\beta(s;p)$ the linear homotopy. To check expected properties and path independence the difference between the potential for a fixed $\mathcal{D}$ are shown as $\Delta\Phi \equiv \Phi_1 - \Phi_2$. The fixed point is a $p = 0$ and the limit cycle at $p = 1$.

will check whether, a), the potential properties, and b), the path independence are fulfilled.

We begin with b). For this purpose we look at the potentials Φ depicted in Fig. 5.6 for different values of $\mathcal{D}$. We see that all potential curves start in the origin at the fixed point and decrease up to $p = 1$, where the limit cycle is located. The potentials of the linear homotopy show the expected minimum at the limit cycle. The ones of the cycle-constant β family also have a minimum there but not as pronounced as for the linear homotopy family.

This directly leads us to the check of b), the path independence. As we see the potential (for one $\mathcal{D}$) have significantly different slopes and hence do not match at the critical point of the limit cycle. If we look at differences in the potential, $\Delta\Phi$, in Fig. 5.6, we can observe that $\Delta\Phi$ looks like a negative sine curves with different amplitudes $\mathcal{D}$. The potential differences vanish before the limit cycle and reach a maximum at the limit cycle, $p = 1$.

Chapter 6

Discussion and Outlook

In order to test a candidate ansatz for a NESS potential we have performed the cycle decomposition of two dynamical systems, namely the van-der-Pol oscillator and Brusselator. We constructed dynamical systems DS($\mathcal{L}$), augmented by isotropic noise, whose orbits are solely cycles. See the cycle families in Fig. 5.1 and 5.4.

For our purpose we need to determine transition rates v between neighboring cycles. To find these we introduced the crosswind operator $\mathcal{R}$ and the closing angle β. To create families of cycles we used different methods, i.e., the cycle-constant crosswind operator and linear homotopy.

We disucssed in Chapter 5 the numerical results of a candidate ansatz for a NESS potential. We see in Figs. 5.3 and 5.6 that the potentials fulfill the expected property, that is, that they are extremal on the invariant manifolds. Furthermore, the potentials are repelling for the unstable fixed point and attracting for the stable limit cycle. On the other hand we checked whether the potentials are independent of the path taken in the cycle space, which is what we expect from the condition of detailed balance of the fluxes between the cycles.

For the van-der-Pol oscillator this can be qualitatively seen as verified, since compared to the numerical values at the minimum, the potential differences can be seen as small. For the Brusselator we saw significant differences between the potentials of the different families at the minimum. Hence, the path independence cannot be verified. We now want to discuss possible reasons for that differences.

The non-zero differences at the limit cycles could be the result of several assumptions and simplifications we made. Since, in this thesis we want to do a first test of our ansatz we have tried to reduce complexity as much as possible. For example, we assumed an isotropic diffusion tensor, which may be artificial and not physical but simplifies the equations. Furthermore, we use arbitrary values for the diffusion constants $\mathcal{D}$, since there is no well-defined temperature in our nonequilibrium setting to relate to. We note that a large value of $\mathcal{D}$ ($\mathcal{D} \geq 10^{-2}$) numerical instabilities are observed in the calculation of the potential. These instabilities need to be solved if

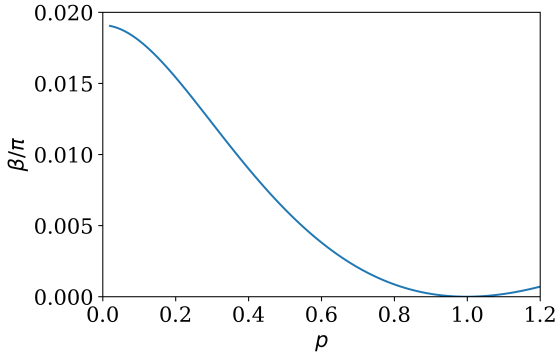

Figure 6.1: Squared closing angle β of the Brusselator for the cycle-constant crosswind angle family. This quantity already shows the extremal property of a potential for invariant manifolds.

one wants to seek a robust definition of a NESS potential. Also there are some numerical challenges for the integration. See for example the cycle-constant crosswind family of the Brusselator (Fig. 5.4) shows a high density of cycles in some regions, which leads to instabilities. For further investigations one the Brusselator one would need to use a integrator, which is capable of high-precision integration.

To conduct further exploration of our ansatz, and give a reliable answer to the question if our ansatz leads to a NESS potential one should also test it for systems with different topology. In addition, one should also evaluate more paths through the cycle space. A possible way of constructing them would be to define a specific cycle in between the invariant manifolds and use linear homotopy to deform cycles from the one invariant manifold onto the given cycle and then again use homotopy to deform the cycles from the given cycle to the other manifold.

Nevertheless, we argue that the realization of the properties expected of a potential may be evidence for the existence of a potential based on the presented ansatz. If the equation derived in Sec. 3.2.1 turn out not to be the desired equations for a NESS potential, we would like to draw the attention to another view of the crosswind: we could think of the closing angle as kind of expressing 'how much force' is needed to deform orbits to cycles. If we integrate this 'force' or find some expression $F(\beta)$ that may gives us a potential, which fulfills the expected properties of a potential. If we, for example, take the simplest function, which is $F(\beta) = \beta^2$, we immediately find this to be a quantity that gains extrema in the invariant manifolds. See for instance Fig. 6.1, where we show the squared closing angle for the cycle-constant crosswind of the Brusselator.

Another simplifying assumption that we need to address in the future is that so far we have restricted ourselves to two-dimensional dynamical systems. In two dimension the Poincaré-Bendixon theorem holds and hence invariant manifold are simple combinations of fixed points, limit cycles and orbits connecting fixed points. For higher dimensions this is not true and there can be more complicated structures, e.g. strange attractors. Furthermore, a single closing angle β would not be sufficient anymore and hence the crosswind operator needs to be redefined.

To summarize, identification of a NESS potential still remains a challenging task. The presented ansatz shows encouraging, albeit not conclusive, evidence that there is hope to find a NESS potential based on our ansatz, or a related one.

Bibliography

[1] B. Altaner, S. Grosskinsky, S. Herminghaus, L. Katthän, M. Timme, and J. Vollmer, *Network representations of nonequilibrium steady states: Cycle decompositions, symmetries, and dominant paths*, Physical Review E **85**, 041133 (2012).

[2] H. Hinrichsen, *Non-equilibrium critical phenomena and phase transitions into absorbing states*, Advances in Physics **49**, 815 (2000).

[3] T. Vicsek and A. Zafeiris, *Collective motion*, Physics Reports **517**, 71 (2012).

[4] T. Speck, *Collective behavior of active brownian particles: From microscopic clustering to macroscopic phase separation*, The European Physical Journal Special Topics **225**, 2287 (2016).

[5] M. E. Cates and J. Tailleur, *Motility-induced phase separation*, Annual Review of Condensed Matter Physics **6**, 219 (2015).

[6] C. Battle, C. P. Broedersz, N. Fakhri, V. F. Geyer, J. Howard, C. F. Schmidt, and F. C. MacKintosh, *Broken detailed balance at mesoscopic scales in active biological systems*, Science **352**, 604 (2016).

[7] S. Herminghaus and M. G. Mazza, *Phase separation in driven granular gases: exploring the elusive character of nonequilibrium steady states*, Soft Matter **13**, 898 (2017).

[8] H. Ozawa, S. Shimokawa, and H. Sakuma, *Thermodynamics of fluid turbulence: A unified approach to the maximum transport properties*, Physical Review E **64**, 026303 (2001).

[9] H. Risken, *The Fokker-Planck Equation*, (Springer 1996).

[10] G. Nicolis and I. Progogine, *Self-Organisation in Nonequilibrium Systems. From Dissipative Structures to Order through Fluctuations.*, (John Wiley & Sons 1977).

[11] R. K. P. Zia and B. Schmittmann, *Probability currents as principal characteristics in the statistical mechanics of non-equilibrium steady states*, Journal of Statistical Mechanics: Theory and Experiment **2007**, P07012 (2007).

[12] M. R. Evans, Y. Kafri, H. M. Koduvely, and D. Mukamel, *Phase separation and coarsening in one-dimensional driven diffusive systems: Local dynamics leading to long-range hamiltonians*, Physical Review E **58**, 2764 (1998).

[13] X.-J. Zhang, H. Qian, and M. Qian, *Stochastic theory of nonequilibrium steady states and its applications. part i*, Physics Reports **510**, 1 (2012).

[14] H. B. Callen, *Thermodynamics and an introduction to thermostatistics*, (Wiley 1985).

[15] W. Grimus, *Statistische Physik und Thermodynamik. Grundlagen und Anwendungen.*, (Berlin: De Gruyter 2015).

[16] N. G. Van Kampen, *Stochastic processes in physics and chemistry*, vol. 1, (Elsevier 1992).

[17] R. Graham and H. Haken, *Generalized thermodynamic potential for markoff systems in detailed balance and far from thermal equilibrium*, Zeitschrift für Physik A Hadrons and nuclei **243**, 289 (1971).

[18] G. N. Lewis, *A new principle of equilibrium*, Proceedings of the National Academy of Sciences of the United States of America **11**, 179 (1925).

[19] J. Schnakenberg, *Network theory of microscopic and macroscopic behavior of master equation systems*, Reviews of Modern Physics **48**, 571 (1976).

[20] R. Landauer, *Inadequacy of entropy and entropy derivatives in characterizing the steady state*, Phys. Rev. A **12**, 636 (1975).

[21] D. J. Griffiths, *Introduction to Electrodynamics*, (Pearson 2013), 4th edition ed.

[22] S. H. Strogatz, *Nonlinear dynamics and chaos: with applications to physics, biology, chemistry, and engineering*, (Westview press 1994).

[23] C. Robinson, *Dynamical Systems: Stability, Symbolic Dynamics, and Chaos*, (CRC Press 1999).

[24] J. Argyris, G. Faust, M. Haase, and R. Friedrich, *Die Erforschung des Chaos*, Springer complexity, (Springer Berlin Heidelberg 2017).

[25] J. Guckenheimer and P. J. Holmes, *Nonlinear oscillations, dynamical systems, and bifurcations of vector fields*, *Applied Mathematical Sciences*, vol. 42, (Springer Science+Business Media 1983).

[26] J. M. Lee, *Introduction to smooth manifolds*, (Springer Science+Business Media 2013).

[27] K. Königsberger, *Analysis 2*, Springer-Lehrbuch, (Physica-Verlag 2004).

[28] L. Perko, *Differential Equations and Dynamical Systems*, Texts in Applied Mathematics, (Springer New York 2001).

[29] O. Penrose, *Foundations of Statistical Mechanics: A Deductive Treatment*, Dover Books on Physics, (Dover Publications 2005).

[30] P. E. Kloeden and E. Platen, *Numerical solution of stochastic differential equations.*, (Berlin: Springer-Verlag 1992).

[31] S. Herminghaus, *Classifying non-equilibrium steady states via invariant manifolds* Private communication (2017).

[32] M. Ruth and B. Hannon, *The Brusselator*, 77–81, (Springer New York, New York, NY 1997).

[33] L. Arnold, G. Bleckert, and K. R. Schenk-Hoppé, *The Stochastic Brusselator: Parametric Noise Destroys Hoft Bifurcation*, (Springer New York, New York, NY 1999).

[34] J. Dormand and P. Prince, *A family of embedded runge-kutta formulae*, Journal of Computational and Applied Mathematics **6**, 19 (1980).

[35] E. Haier, N. S., and G. Wanner, *Solving Ordinary Differential Equations I. Nonstiff Problems*, (Springer Berlin Heidelberg 1987).

Appendix

A.1 Fokker-Planck equation

A.1.1 Fokker-Planck equation in higher dimensions

A Fokker-Planck equation for n variables $x = (x_1, \ldots, x_n)^{\mathrm{T}} \in \mathbb{R}^n$ reads

$$\frac{\partial p}{\partial t}(x,t) = \left[-\sum_{i=1}^{n} \frac{\partial}{\partial x} \mathcal{K}_i(x,t) + \sum_{i,j=1}^{n} \frac{\partial^2}{\partial x^2} \mathcal{D}_{ij}(x,t) \right] p(x,t), \tag{A.1}$$

where $\mathcal{K}_i$ is the drift vector and $\mathcal{D}_{ij}$ the diffusion tensor. See Sec. 2.3.3 for further reading.

A.1.2 Drift and Diffusion constant from Langevin equation

Consider the Langevin equation for a n-dimensional system with state vector $X = (X_1, \ldots, X_n)$, which has the general form

$$\dot{X}_i = a_i(X,t) + b_{ij}(X,t)\Gamma_j(t), \tag{A.2}$$

with a the deterministic dynamics, b the noise terms and Γ Gaussian white noise. This is a n-dimensional SDE, see Eq. (2.30). Note that we use Einsteins' sum convention here. This drift $\mathcal{K}$ and diffusion constant $\mathcal{D}$ are then given by [9]

$$\mathcal{K}_i(X,t) = a_i(X,t) + b_{kj}(X,t)\partial_k b_{ij}(X,t) \tag{A.3}$$

$$\mathcal{D}_{ij}(X,t) = b_{ik}(X,t)b_{jk}(X,t). \tag{A.4}$$

For additive noise, i.e., when $b = b(t)$, the derivative and hence second term in Eq. (A.3) vanishes and a corresponds to our dynamical system f as in Sec. 2.2. If the second term does not vanish, we call it *noise-induced drift* [9].

A.2 Master equation

The transition probability p_2 (see Sec. 2.3.1) can be rewritten into transitions per unit time $w(x'|x;t)$,

$$p_2(x, t+\tau|x', t) = [1 - a(x,t)\tau]\, \delta(x - x') + w(x|x';t)\tau + O(\tau^2), \tag{A.5}$$

with

$$a(x',t) = \int w(x'|x;t)\mathrm{d}x. \tag{A.6}$$

Acknowledgements

Special thanks to Marco G. Mazza for the encouragement and support. The author thanks Stephan Herminghaus and Prakhar Godara for the inspiring discussions and numerous helpful hints. Also the author thanks the MPIDS for their helpfulness. Furthermore, the author thanks his family and friends for the support over the whole time.

Erklärung

Gemäss §12(9) der Prüfungsordnung des Studiengangs Physik an der Universität Göttingen:

Hiermit erkläre ich, dass ich diese Abschlussarbeit selbständig verfasst habe, keine anderen als die angegebenen Quellen und Hilfsmittel benutzt habe und alle Stellen, die wörtlich oder sinngemäss aus veröffentlichten Schriften entnommen wurden, als solche kenntlich gemacht habe. Darüber hinaus erkläre ich, dass diese Abschlussarbeit nicht, auch nicht auszugsweise, im Rahmen einer nichtbestandenen Prüfung an dieser oder einer anderen Hochschule eingereicht wurde.

Des Weiteren versichere ich, dass die schriftliche Version dieser Abschlussarbeit mit der ergänzend vorgelegten Version übereinstimmt.

Göttingen, den 14. Februar 2018

(Jens Lucht)